Leaching of Phosphorus from Biomass Ash and Model Chemicals

Thesis for M.Sc. in Chemistry

by

Johanna Clayhills

Laboratory of Molecular Science and Engineering

Faculty of Science and Engineering

Åbo Akademi University

January 2024

Title of the thesis:	Leaching of Phosphorus from Biomass Ash and Model Chemicals
Author:	Johanna Clayhills
Thesis supervisors:	Dr Daniel Schmid *Åbo Akademi University, Turku, Finland* Dr Emil Vainio *Åbo Akademi University, Turku, Finland* Prof. Leena Hupa *Åbo Akademi University, Turku, Finland*

Abstract

Phosphorus is an important raw material used mainly in fertilizers, with population growth increasing the demand. Sustainable sources of phosphorus are investigated to prevent the depletion of phosphorus reservoirs. While ashes have long served as fertilizers, they often contain heavy metals, and methods to prevent contamination are crucial for environmental health. Leaching of ashes before usage can extract the useful components and separate them from the harmful ones. This thesis focuses on exploring the leaching behaviours of phosphates from both model chemicals and biomass ash. Additionally, it introduces an alternative analytical method for determining phosphorus concentrations in complex aqueous solutions.

The research presented in this thesis delves into the molybdenum blue method's accuracy and its application to determine the phosphorus leaching from biomass ashes in diverse solvents. The experimental procedure investigated single phosphates and phosphate mixtures, as well as hydroxyapatites, which are present in biomass ashes, providing a fundamental understanding of phosphorus leaching. Solvents are employed to adjust pH, revealing a correlation between lower pH levels and increased phosphorus leaching, a trend also seen in equilibrium data. Finally, studying the leaching of biomass ashes stepwise, first in ultrapure water and then in either HCl or HNO3, revealed no significant difference in the choice of acid.

Furthermore, the reliability of the molybdenum blue method with Sb(III) and ascorbic acid as reagents, for simple and complex samples was evaluated. All samples underwent analysis using the molybdenum blue method. The biomass ash results obtained from this method were then compared with those obtained from ICP-OES. The values were comparable but due to issues with the sensitivity of ICP-OES, some uncertainty remains. Additionally, the outcomes from ICP-OES and SEM-EDX reveal that the failure to analyze wheat bran using the molybdenum blue method was most likely due to interferences.

The concentration of phosphorus in biomass ashes, determined through the molybdenum blue method, shows potential as an alternative to ICP-OES for rapid

phosphorus concentration estimates, but caution is warranted due to potential interferences making the molybdenum blue method unreliable.

Keywords: Phosphorus, phosphorus analysis, biomass ash leaching, molybdenum blue method.

Acknowledgement

This master's thesis has received funding from the Research Council of Finland financed project "High temperature chemistry of phosphorus – pathways to more effective recycling and utilization" (PhosPath), decision number 341405.

I would like to express my gratitude to my supervisors, Daniel Schmid, Emil Vainio, and Leena Hupa, for their guidance and support during this thesis. I also want to thank everyone from the Inorganic Chemistry group for their assistance in the lab and friendliness towards me.

A heartfelt thanks to my dad for his unwavering support and to my friends for their encouragement throughout this journey. Their support means the world to me, and I could not have done this without them.

Johanna Clayhills
Åbo, 16th January 2024

Abbreviations

12-MPA	12-molybdophosphoric acid
CFB	Circulating fluidized bed
HSAB	Hard and soft acids and bases
ICP-OES	Inductively coupled plasma optical emission spectroscopy
L/S	Liquid-to-solid
MB	Molybdenum blue
MBM	Meat and bone meal
PMB	Phosphomolybdenum blue
RSC	Rapeseed cake
SEM-EDX	Scanning electron microscope with energy dispersive X-ray spectroscopy
SSS	Sunflower seed shell
UV-Vis	Ultraviolet and visible light
WB	Wheat bran

Table of Contents

List of Figures

List of Tables

1 Introduction

Phosphorus is among the critical raw materials important to the European Union, playing a pivotal role in Europe's economy and development. Materials containing phosphorus are integral to various sectors, contributing significantly to industrial processes, agriculture, and technological advancements within the region. However, concerns are rising as the supply of certain raw materials is being depleted [1] and the demand is rising as a result of population growth. As the population continues to grow, so does the demand for food. This increase has led to a corresponding rise in the use of fertilizers, which often contain phosphorus as a key ingredient.[2] In 2022, fertilizer prices surpassed those seen during the 2008 global financial crisis due to factors such as higher energy costs, supply limitations,[3,4] the conflict between Ukraine and Russia, and trade restrictions in China. The prices have since decreased, although they have not yet returned to the levels seen before 2022.[4] Phosphorus, primarily found in phosphate rock as the mineral apatite [$Ca_{10}(PO_4)_6$(F, Cl, or $OH)_2$], serves as a crucial component in the production of fertilizers, making it essential for agriculture.[5,6] Additionally, about 10% of phosphorus is used in the production of animal feed supplements, with 5% used in chemical industries, food additives,[7] batteries/energy conversion and storage.[8,9] In 2022, global phosphate rock mining reached 220 million metric tons.[10] One-fifth of the phosphorus produced is consumed by humans with the rest used in industries and some inevitably going to waste.[11] Moreover, the increased use of phosphorus raises concerns about the depletion of the Earth's non-renewable phosphate rock reserves,[5] which are estimated to be around 72,000 million metric tons[10] and will be depleted in 50-100 years.[11] Morocco alone holds 70% of the world’s phosphate rock reserves.[10]

All of this has increased the necessity of finding new sustainable phosphorus sources. One possible source is ashes produced from the thermal conversion of phosphorus-rich feedstocks. These ashes may be used as fertilizer, but this poses a problem, as some ashes contain heavy metals that may leach along with phosphorus, leading to potential accumulation in the surrounding soil or waterways.[11,12] Therefore, studies to selectively remove heavy metals, phosphorus, and other contaminants from each other have been researched. The leaching of phosphorus has been investigated for various

waste streams, e.g., sewage sludge, meat, bone meal, etc.[13–17] One source of phosphorus is agricultural residues which are widely available resources in many parts of the world. However, the high phosphorus and alkali content in agricultural residues can cause agglomeration and defluidization during thermal conversion.[18] Improving the understanding of phosphorus leaching from ashes produced through the combustion of phosphorus-rich residues has been researched in this thesis in the pursuit of finding a sustainable phosphorus resource. Finding new phosphorus resources can contribute to a more sustainable planet. New phosphorus resources would minimize environmental contamination and the depletion of phosphorus reserves as well as maximize the efficient utilization of biomass waste.

2 Literature Review

2.1 Phosphorus

Phosphorus is a chemical element represented by the letter P found in group 15/5A on the periodic table with an atomic number of 15.[5,19] It is the 12th most abundant element in Earth's crust and a majority of phosphorus is found in nature as phosphate ions (PO_4^{3-}). The phosphorus cycle (Figure 1) showcases the movement of phosphorus through various reservoirs and clarifies why our phosphorus sources will diminish over time, despite the overall phosphorus quantity remaining constant. Compared to the carbon, nitrogen, and sulphur cycles, the phosphorus cycle lacks a gaseous compound and comprises as solid and aqueous form in the environment.[20]

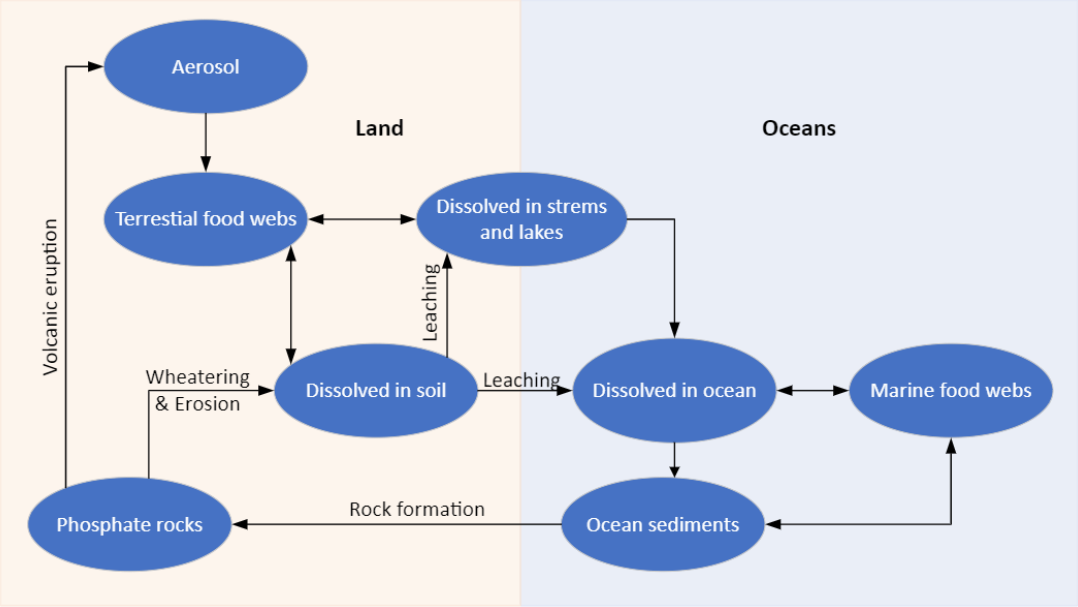

Figure 1. Simplified schematic diagram of the phosphorus cycle.[20,21]

Most phosphorus is found in rock and sedimentary deposits, and these reserves are gradually released into the environment through weathering, leaching, and mining activities. The phosphorus is bound in minerals, with apatite ($Ca_5(PO_4)_3(F, Cl, OH)$) being the most abundant, which encompasses hydroxyapatite, fluorapatite, and chlorapatite. Table 1 lists various phosphate-containing minerals. Phosphate minerals typically originate from magmatic processes or precipitation from solution. The resulting chemical composition varies based on the ions present during mineral

formation, leading to heterogeneous deposits known as 'phosphorites' that encompass diverse phosphate mineral types.[20]

Table 1. Phosphate minerals and their chemical compositions. Apatite is the general term for the three minerals hydroxyapatite, fluorapatite, and chlorapatite [20]

Mineral	Chemical composition
Apatite	$Ca_5(PO_4)_3(F,Cl,OH)$
Hydroxyapatite	$Ca_5(PO_4)_3OH$
Fluorapatite	$Ca_5(PO_4)_3F$
Chlorapatite	$Ca_5(PO_4)_3Cl$
Frankolite	$Ca_{10-a-b}\ Na_aMg_b(PO_4)_{6-x}(CO_3)_{x-y-z}(CO_3F)_y(SO_4)_zF_2$
Lazulite	$(Mg,Fe)Al_2(PO_4)_2(OH)_2$
Monazite	$(Ce,La,Y,Th)PO_4$
Pyromorphite	$Pb_5(PO_4)_3Cl$
Strengite	$FePO_4 \cdot 2H_2O$
Triphylite	$Li(Fe,Mn)PO_4$
Turquoise	$CuAl_6(PO_4)_4(OH)_8 \cdot 5H_2O$
Variscite	$AlPO_4 \cdot 2H_2O$
Vauxite	$FeAl_2(PO_4)_2(OH)_2 \cdot 6H_2O$
Vivianite	$Fe_3(PO_4)_2 \cdot 8H_2O$
Wavellite	$Al_3(PO_4)_2(OH)_3 \cdot 5H_2O$

In both soil and lake sediments, the weathered phosphorus mineral exists as inorganic Phosphorus. Furthermore, the presence of organic phosphorus results from the decomposition, excretion, and cellular breakdown of biological organisms. Phosphorus soil properties and behaviour are influenced by microbial activity, temperature, pH, oxygenation levels, and the presence of elements such as Al, Ca, or Fe in soils.[20] While the soil might contain a high phosphorus content, it is not readily available in plants due to the limited solubility and high-sorption capacity of inorganic Phosphorus, which is the primary form plants absorb.[22] Plants absorb $H_2PO_4^-$ and HPO_4^{2-} from the soil, with the amount present of each compound depending on soil pH. The phosphorus content in plants typically ranges between 0.1 to 0.5 wt%, on dry basis (Figure 2).[23]

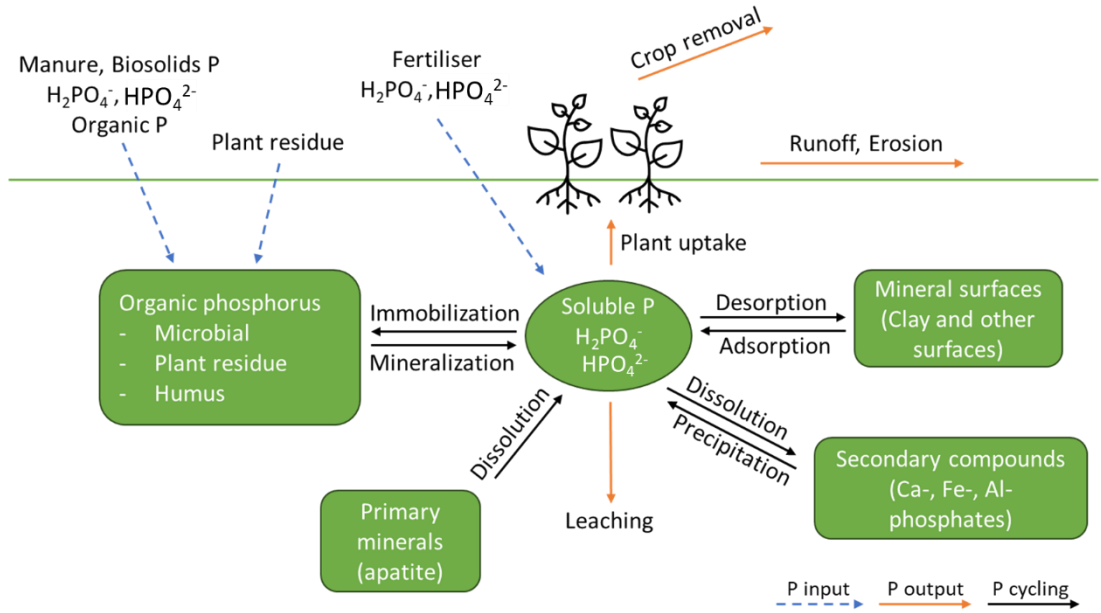

Figure 2. Phosphorus cycling in soil. Internal phosphorus cycling (black lines), input of phosphorus (blue lines), and phosphorus output (orange lines).[23]

Phosphorus is primarily depleted from the soil through harvesting crops and, to a lesser extent, through processes such as soil erosion, runoff, and leaching. Fertilizers can be added to the soil to add usable phosphorus and other nutrients for plants to use to minimize restricted growth and development of plants. However, adding fertilizers to soil can cause other problems, such as overapplication leading to eutrophication. In fertilizers, the amount of available phosphorus for plants includes water-soluble and citrate-soluble Phosphorus. However, the total phosphorus is the sum of available and citrate-insoluble Phosphorus. The water-insoluble and citrate-soluble phosphorus cannot be taken up by plants, at least not in significant amounts.[23]

Most of the phosphorus in plants is found as organophosphates (also known as organic phosphate esters or OPE) and are present as nucleic acid, phosphoproteins, phospholipids, sugar phosphates, and adenosine triphosphate (ATP).[24] For humans and animals, phosphorus is obtained through plants and is an important component in bones, teeth, and cells.[5]

2.2 Leaching

Leaching is the process by which a solute is separated or extracted from a solid material using a solvent as the extracting medium. This process results in either the solid material becoming the desired component, or the solution. The different leaching methods also depend on various factors, including concentration, distribution, intermolecular forces, and size. With an evenly distributed solute in the solid, the surface material will dissolve first, and leave a porous structure, which will become challenging and lower the extraction rate the further into the solid it must reach. If, however, the solid has a high solute content, the porous structure may break down into smaller pieces, effectively increasing the solvent's access to the solute. In this way, the presence of a higher solute content can enhance the leaching process. This process can be divided into three parts: the solute undergoes a phase transition as it dissolves in the solvent, the dissolved solute diffuses through the solid's pores to the outside of the particle, and the solute transfers from the solution in contact with the particles to the main bulk of the solution, completing the leaching process.[15]
Leaching can be used for a variety of reasons, such as the assessment of hazardous or unwanted elements in for example fertilizers and construction materials.[25,26] Additionally, leaching can be used to extract components from a solid, for example, rare earth elements from rocks, batteries,[27] or from sewage waste.[28]

Ashes from the combustion of municipal sewage sludge, MBM, and agricultural residues have a high phosphorus content. This elevated phosphorus concentration is the reason behind the growing interest in utilizing these ashes for their potential as fertilizers.[6] Researchers have conducted studies on various ashes and parameters to identify the biomasses that give favourable results, but experiments with agriculture residue are lacking.[6,13,28–31] The composition of the ash can vary depending on the location from which it is collected, such as in a circulating fluidized bed (CFB) boiler. In general, a significant portion, ranging from 75% to 98% of the phosphorus exits the CFB boiler and becomes retained in the fly ash. Moreover, fly ash tends to exhibit an enrichment of Phosphorus, alongside trace elements.[13] The Phosphorus can then be leached from the fly ash, with numerous studies on biomass ashes revealing that the most favourable outcomes occur when the leaching solution has a pH below 2.[6,13,29]

The pH is lowered with acid and studies using several acids concluded that H_2SO_4 is the best acid considering the economic cost and effectiveness in leaching Phosphorus.[6,13,28–30,32] Since sulfuric acid is a strong oxidizer and tends to create less soluble sulfate complexes of trace metals, it has been utilized in various studies for metal extraction. On the other hand, hydrochloric acid creates soluble complexes with most heavy metals by introducing chloride ions to the leachate. However, it has been shown that hydrochloric acid yields a greater metal concentration than sulfuric acid when leaching metals from sewage sludge, challenging the conventional preference for sulphuric acid in metal extraction process.[6,13,29,31] Another important parameter to consider is the liquid-to-solid (L/S) ratio, as demonstrated by B.K. Biswas et al., where an increase in this ratio was found to correspond with a higher amount of phosphorus released during the leaching process of incinerated sewage sludge ash in both H_2SO_4 and HCl solutions.[29] They also found that the cost-effective acid consumption and complete leaching of phosphorus involves using 0.05 mol/L sulphuric acid with an L/S ratio of 150 mL/g. In addition, for hydrochloric acid, the best conditions were 0.1 mol/L at a L/S ratio of 150 mL/g. This combination at 30 °C for 4 hours of mixing ensures optimal results during the leaching process of phosphorus from incinerated sewage sludge ash.[29] However, to ensure a complete extraction of Phosphorus, leaching was extended to 3 or 4 hours,[6,29] despite 2 hours being observed as sufficient.[29]

3 Aim of this work

The present work investigates the leaching behaviour of Phosphorus from model compounds and real biomass ashes. By examining the leaching behaviour of both single phosphates and phosphate mixtures, the objective was to achieve a comprehensive understanding of Phosphorus leaching from biomass ash. In addition, experimental data from the leaching tests was compared to chemical equilibrium calculations to assess how well the results are in agreement. Simultaneously, the molybdenum blue method for determination of phosphorus concentration was assessed.

4 Methods

4.1 UV-Vis spectrophotometry

UV-VIS spectrophotometry is an analytical technique used to measure the absorption or transmission of ultraviolet (180-390 nm) and visible (390-780 nm) light from a substance. Widely used for quantitative analysis, this method has limitations in identifying substances, as different substances can exhibit similar spectra. Chromophores are functional groups in molecules that can absorb energy. For example, conjugated systems absorb light near the UV region; therefore, molecules with this structure are usually present in a specific range in the spectra. Thus, different compounds with the same chromophores could have very similar UV-VIS spectra, even though they are different. Other chromophores can even alter the UV-VIS spectra, making identifying molecules difficult. The spectra can indicate what kind of building blocks there might be in the molecule but seldom reveal the structure. Instead, UV-VIS spectrophotometry is a method to obtain a quantitative analysis of the amount of known analyte in the solution.[33,34] This is determined by using Beer's Law, which establishes a direct relationship between the concentration of an absorbing substance and the absorption of light. When a substance absorbs light in the UV/visible range, its concentration can be quantitatively measured based on the principles derived from Beer's Law. The absorbance of a substance can be obtained by analysing its spectrum, particularly the height of the absorbance peak. In general, the concentration of the substance is directly proportional to its absorbance, and by applying the absorbance to Beer's Law the concentration can be calculated.[33] It is worth noting that Beer's Law is not valid at high concentrations (>0.01 mol l^{-1}) due to interactions between analyte molecules and limitations due to instrumental and chemical deviations.[34]

The UV-VIS spectra are obtained from a UV-VIS spectrophotometer, which comes in two types: single-beam and double-beam spectrophotometers, the former being cheaper.[34,35] Both spectrophotometers have a radiation source, a wavelength-selection device/monochromator, a sample compartment, a detector, and an output device.[34–36] The most common source for visible radiation in spectrophotometry is a tungsten filament and for UV radiation, a deuterium lamp. A grating monochromator is commonly utilized to achieve the best resolution in wavelength selection. The sample

is put into a cell, which is then put into the sample compartment in the spectrophotometer. Depending on the analysis conducted, three different cell materials are used: glass for wavelength 340 nm or larger, quartz for both UV and visible light, and plastic for the visible. The sample should be taken into consideration when choosing a cell to avoid interaction between sample and cell. The shape of the cell can differ depending on the sample, but the standard is a 10 nm square cell. The detector changes the light transmitted into an electrical signal, with the most commonly used detector being a photomultiplier.[34,36] A double-beam spectrometer differs from a single-beam spectrometer in that it features a chopper between the wavelength-selection device and sample compartment that regulates the radiation path as well as having a sample and blank cell. With a single-beam spectrophotometer, a single beam of light passes through the sample and reaches the detector. The intensity of the light beam is measured before and after it passes through the sample. The instrument compares the absorbance of the sample with a reference blank (solvent or empty cell) to determine the amount of light absorbed by the sample. The light beam is split into two paths in a double-beam spectrophotometer. One path contains the sample, while the other path contains a reference blank. Both beams pass through their respective compartments and reach individual detectors. The instrument simultaneously measures the absorbance of the sample and the reference blank.[33,35]

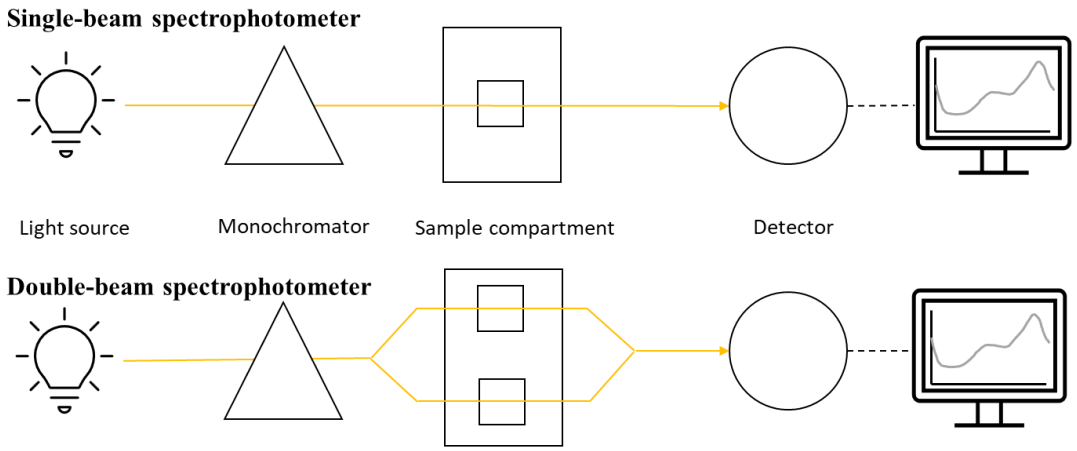

Figure 3. Simplified scheme of a single-beam and double-beam spectrophotometer

4.2 Molybdenum blue method

As the name suggests, the molybdenum blue (MB) method creates a vividly coloured blue molybdenum compound. The first recorded mention of this is found in Carl Wilhelm Scheele's report from 1783. However, J. J. Berzelius is credited with discovering MB (Mo_5O_{14}*nH_2O) and being the first to describe its chemical composition. In 1934, Keggin proposed the structures of 12-heteropoly acids and other reports suggesting that there are several molybdate blue species. When speaking about MB, one usually refers to multiple reduced molybdate species that can include a heteroatom, for example, Phosphorus.[37]

The MB method is a widely used method for assessing water quality as orthophosphate concentrations are a vital water quality parameter.[38] The concentration of silicate, arsenate, and germanate can also be determined using the MB method. Under acidic conditions, phosphate ion and molybdate ion form a heteropoly acid (Equation 1), which is then reduced to form the vividly coloured phosphomolybdenum blue (PMB) species (Equation 2).[37]

$$PO_4^{3-} + 12MoO_4^{2-} + 27H^+ \rightarrow H_3PO_4(MoO_3)_{12} + 12H_2O$$

Equation 1. Formation of heteropolyacid from phosphate ion and molybdate ion.[37]

$$H_3PMO(\text{VI})_{12}O_{40} + Reductant \rightarrow [H_4PMo(\text{VI})_8Mo(\text{V})_4O_{40}]^{3-}$$

Equation 2 Reduction of a heteropolyacid to phosphomolybdenum blue (PMB) species.[37]

Both the synthesis of the heteropoly acid and the management of its reduction depend on the quantities of acid and molybdate. Orthophosphate PO^{3-}_4 generates Keggin ions $[X^{n+}Mo_{12}O_{40}]^{(8-n)-}$, where X is the heteroatom. This species is known as 12-molybdophosphoric acid (12-MPA) in the case of orthophosphate.[39] Furthermore, orthophosphate determination techniques work best when performed at a pH range of 0 to 1, giving the best colour intensity because it forms suitable amounts of stable reduced product without excessive direct reduction of Mo(VI). It requires a strong acid such as H_2SO_4 or HCl, with the former being the prevalent choice of acid, despite its potential limitations, but depending on the conditions HCl is also a viable alternative.

The reduction of 12-MPA leads to the formation of PMB species and is affected by pH, reductants, temperature, time, and interfering ions. The use of reductants has a big impact on MB chemistry and therefore an important part to discuss, since it also alters the appearance of the UV-Vis spectra. The most commonly used reductants are Sn(II), ascorbic acid, and a mixture of ascorbic acid with Sb(III). The former rapidly reduces 12-MPA, while the combination of Sb(III) and ascorbic acid speeds up the reduction, which is otherwise kinetically slow without ascorbic acid. Depending on heating and acidity $SnCl_2$ can form $Sn_2PMB(4e^-)$, $SnPMB(4e^-)$, and $PMB(4e^-)$; non-metallic reductants form $PMB(4e^-)$, $PMB(2e^-)$; and non-metallic reductant and Sb(III) form $Sb_2PMB(4e^-)$. All these PMB species' spectral features can look different depending on the reductant as well as the amount of acid, reductant, and molybdenum present (Figure 4).[37]

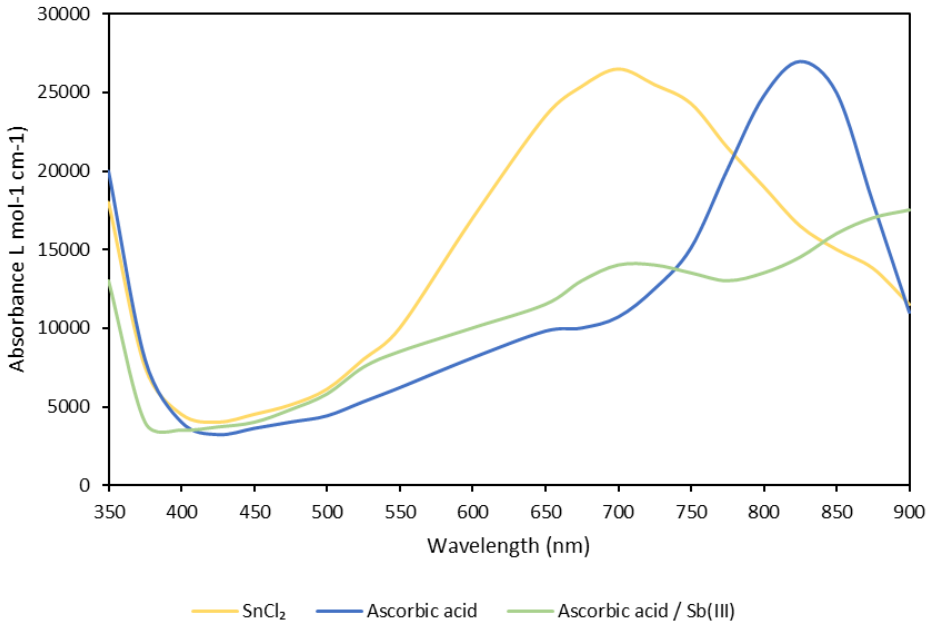

Figure 4. Comparison of product spectra for three commonly used reductants in MB methods: $SnCl_2$ (yellow line), ascorbic acid (blue line), and ascorbic acid with Sb(III) (green line). Each solution contained the same amount of orthophosphates.[37]

The reductants used for this thesis were ascorbic acid and Sb(III) mixture (see *5.2.4 Molybdenum blue procedure*) and that is why the discussion below focuses on it instead of other reductants. By using ascorbic acid and Sb(III) the reduction of 12-MPA can be achieved in 10 minutes, eliminating the need for extensive heating procedures, while also yielding a stable product lasting several hours and is not

affected by chloride interference.[37] Figure 5 provides a visual representation of the spectra for 1, 2, and 5 ppm concentrations when employing ascorbic acid and Sb(III) as reductants. The figure illustrates the variations in spectra based on concentration. However, it is important to note that when utilizing ascorbic acid and Sb(III) for the reduction reaction, the temperature should not exceed 35 °C as it will show a lower concentration of the measurable PMB species and therefore give inaccurate results.[37,40]

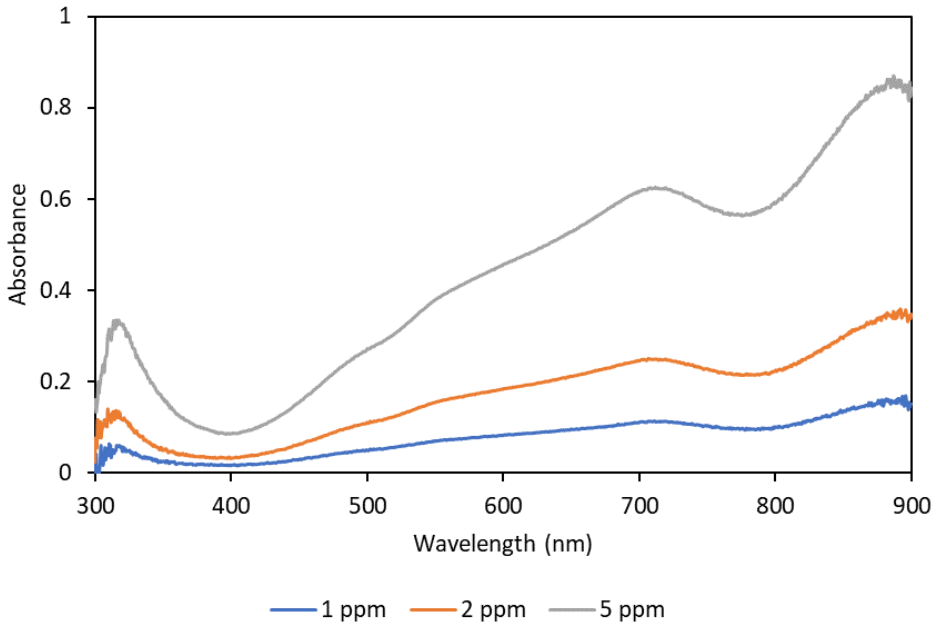

Figure 5. Spectral variations at concentrations of 1, 2, and 5 ppm using ascorbic acid and Sb(III) as reductants.

An accurate determination of the analyte is preferred and vital for numerous applications, but interferences can impact the reliability and precision of results. The interferences can underestimate or overestimate the amount of analyte in the solution. By understanding the interferences, they can be avoided or worked around. The interferences encountered in MB methods can be divided into three categories: additive, subtractive, and multifunctional interferences.

Additive interferences refer to the other analytes that can react with the molybdate instead of the desired analyte. In the context of the thesis, arsenate or silicate, instead of Phosphorus, can form with molybdate a reducible heteropoly acid, and therefore, give inaccurate results of the desired analyte concentration.

Subtractive interferences are organic acid or fluoride that can inhibit MB reaction, and chloride that can decrease the analytical signal. The chloride interference, also called

'salt error', is difficult as the degree of sensitivity differs depending on the concentration of Cl^- and orthophosphates present.
Multifunctional interferences can present both additive and subtractive interferences, for example, sulphide which in low phosphorus concentrations causes additive interferences and in high phosphorus concentrations causes subtractive interference.
By selecting a suitable acid and reductant for the regarding sample, interferences can be avoided, and accurate results can be obtained.

4.3 ICP-OES

Inductively coupled plasma-atomic emission spectrometry (ICP-OES) is an analytical technique used for elemental analysis in various samples.[41] ICP-OES is applied in various applications such as food, agriculture, drug, and geological studies or analyzes. Compared to other spectrometric techniques ICP-OES has higher sensitivity, lower detection limits, less chemical interference, and is less time consuming. ICP-OES ensures reliable, accurate, and reproducible results with continuous wavelength coverage, which provides dynamic range and reduces interference. The ICP-OES principle is based on the use of high-temperature plasma to ionize and excite atoms, followed by the measurement of the emitted light as these excited atoms return to their ground state. This emitted light is then analyzed to determine the elemental composition and concentration within the sample.[42]

Liquid or gas samples are mixed with argon gas and a nebulizer spays it as fine aerosol particles into a spray chamber. The bigger particles are removed in the spray chamber, whereas the smaller aerosols continue to the plasma torch. Solid samples need to be liquified before going to the nebulizer, either by extraction or acid digestion. The aerosol is moved to the plasma torch with another stream of argon gas. The plasma torch compromises three concentric glass tubes with the argon gas and the sample flowing through the inner tube. The outer and middle tube flows with argon gas that sustains the plasma temperature of 8000–10000 K. A magnetic field is produced by an electric current flowing through a metal coil that surrounds the glass from a radio frequency generator. All of this creates the plasma when it has been ignited. Heat

breaks down the sample molecules into atoms and ions, supplying the energy needed to excite the atoms' and ions' electrons and raise their energy levels. The emitted light/photons from an electron returning to a lower level are collected with a concave mirror or lens and then captured on a wavelength selection device for example a monochromator. The wavelengths are then converted into an electrical signal by a photodetector.[41,42]

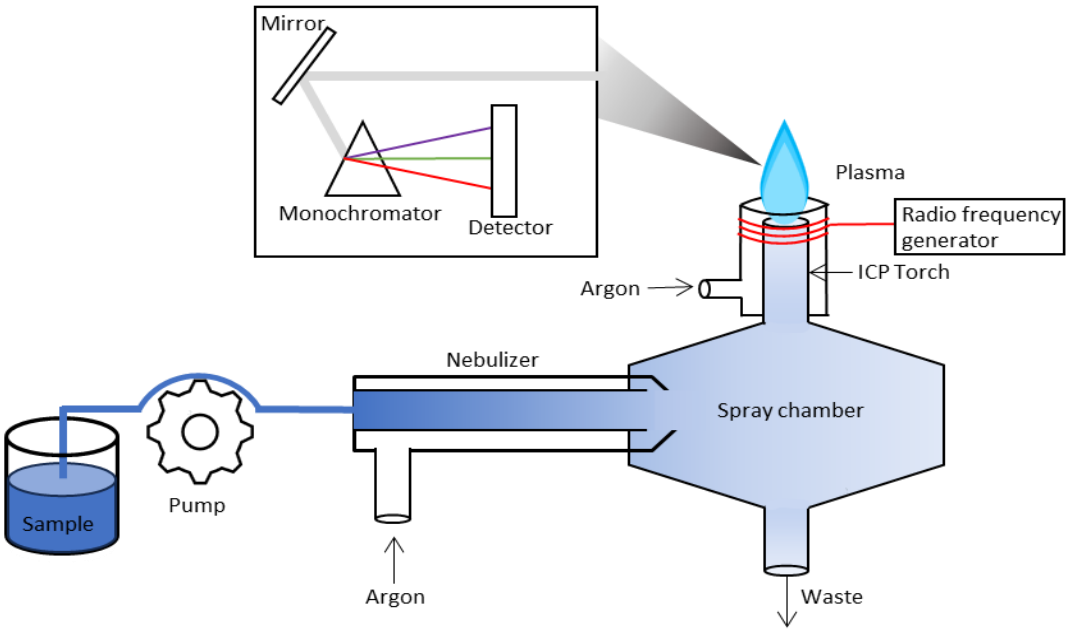

Figure 6. Simplified scheme of the basic operational principles of ICP-OES.[41,42]

4.4 SEM-EDX

Scanning electron microscopy with energy dispersive X-ray spectroscopy (SEM-EDX) is a technique for material characterization, allowing surfaces to be observed at submicron and nano-level to provide information about the surface, composition, and defects in bulk materials. By using an electron beam, SEM-EDX enlarges small features or objects invisible to the human eye. The focused electron beam hits the surface of the solid, interacts with its atoms and generates a variety of signals that are collected to form an image of the sample (Figure 7). Detectors collect secondary and backscattered electrons, as well as characteristic X-rays, yielding information on attributes such as composition, morphology, grain size and shape, grain boundaries,

and more. Within SEM-EDX instrumentation, multiple components, including the lenses, contribute to the overall image formation process. These components allow SEM-EDX to achieve remarkable image resolutions, as fine as 1 nm, in contrast to the human eye's resolution of 200 µm and the 0.2 µm resolution provided by light microscopes. Additionally, the anode near the electron gun facilitates the generating, focusing, and controlling of the electron beam. The strengths of SEM-EDX include a wide range of advantages, including the examination of diverse specimens, rapid imaging and analysis, suitability for dry and wet samples, cost-effectiveness, availability compared to pricier alternatives, etc. However, SEM-EDX has its limitations, including size restrictions, exclusive applicability to solid samples, incapability of detecting elements such as H, He, or Li using an EDS (Energy-Dispersive X-ray Spectroscopy) detector, and the requirement to examine samples under vacuum conditions.[43]

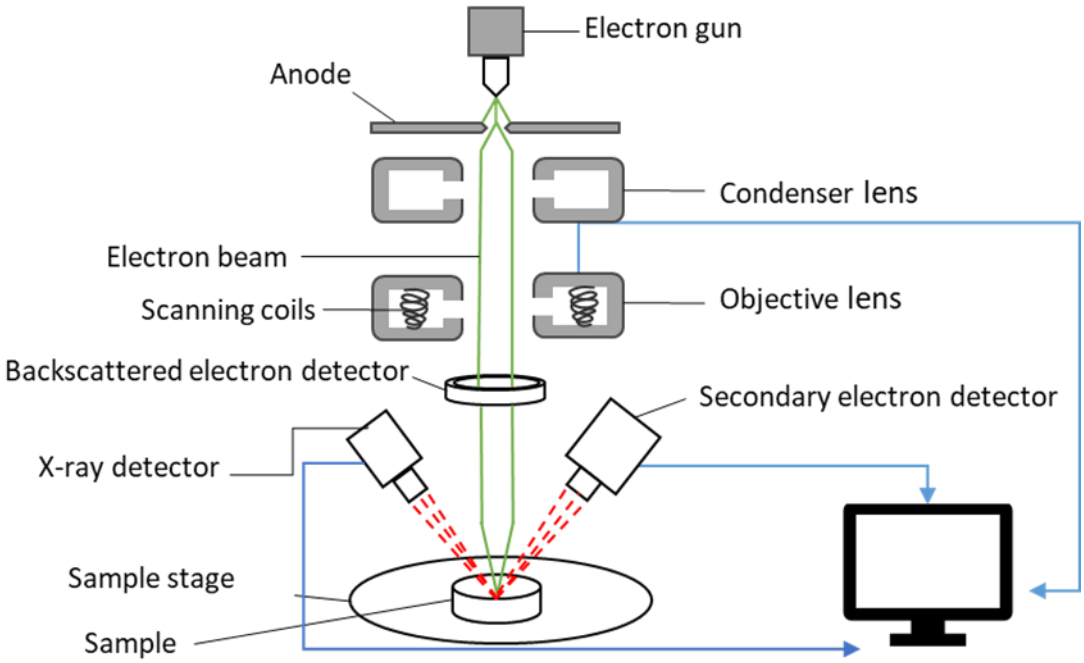

Figure 7. Simplified scheme of the basic principles of the electron column and specimen chamber of the SEM-EDX.[43]

4.5 Factsage

The FactSage Software was used for chemical equilibrium calculations. Factsage is an integrated database computing system in chemical thermodynamics, which uses Gibbs energy minimization. It can be used to calculate complex phase equilibria in systems and stimulate the dynamics of reactors or processes.[44] Gibbs free energy is a thermodynamic potential that helps to predict the spontaneity and feasibility of a process. Gibbs free energy, G, is defined in Equation 3 where H is enthalpy, T is temperature (in Kelvin), and S is entropy. If ΔG is negative the process is spontaneous, if it is positive the process is non-spontaneous, and if it is zero the system is at equilibrium.[19]

$$\Delta G = \Delta H - T\Delta S$$

Equation 3. Gibbs free energy.[45]

Gibbs energy minimization is a classical approach in thermodynamics for equilibrium calculations in chemical reactions.[46] Equation 4 represents the overall function of temperature, pressure, and product mole composition. In the equation n_i stands for moles, P_i for gas partial pressure, X_i for mole fraction, γ_i for activity coefficient, and g_i^o for standard molar Gibbs energy. The second row represents the pure condensed phases, the third row solution 1, the fourth row solution 2, and the last row the next solutions.[45]

$$G = \sum n_i(g_i^0 + RT\ln P_i)$$
$$+\sum n_i g_i^\circ$$
$$+\sum n_i(g_i^\circ + RT\ln X_i + RT\ln\gamma_i)$$
$$+\sum n_i(g_i^\circ + RT\ln X_i + RT\ln\gamma_i)$$
$$+\cdots$$

Equation 4. Gibbs energy minimization [45]

5 Experimental Section

5.1 Material, instruments, and chemicals

The elemental analysis of biomass ashes was conducted using an Inductively Coupled Plasma Optical Emission Spectrometer (ICP-OES), specifically the PerkinElmer Optima 5300 DV model. This instrument allows for precise and simultaneous measurement of various elements in the samples.

High-temperature treatments were performed using a Nabertherm Muffle Furnace, model LT 24/11/P330. This furnace provided controlled heating conditions essential for hydroxyapatite synthesis.

The structural and elemental analyses of biomass ashes were carried out using Scanning Electron Microscopy coupled with Energy Dispersive X-ray Spectroscopy (SEM-EDX). The equipment utilized was a Leo Gemini 1530 with a Thermo Scientific UltraDry Silicon Drift Detector, providing detailed insights into the composition of the samples.

The Shimadzu UV-2501PC UV Spectrometer, manufactured by Shimadzu, played a crucial role in accurately measuring absorbance and concentration in the UV-visible range (190 to 900 nm). This instrument was essential for quantifying phosphates in liquid samples, following a DGT research-based method.

Filtration processes used Whatman Grade 40 Ashless Filter Paper with a diameter of 90 mm. The filter paper has a medium nominal particle retention rating of 8 µm. This filter paper was selected for its high purity and compatibility with the experimental requirements.

For the equilibrium calculations Factsage 8.1 was used utilizing the FactPS database for pure substance and FTHelg for aqueous solute species. The calculations were performed for 20 °C and 1 atm.

Listed in Table 2 are the different chemicals used during the experimental part of this work. Along with the solvents, the quality grade and the manufacturer of the chemical are listed. Water used in the experiments was synonymous with ultrapure water.

Table 2. Chemicals used during the experiments

Chemical	**Quality grade**	**Manufacturer**
Aluminium phosphate	Reagent grade	Sigma-Aldrich
Buffer Solution	Potassium hydrogen phthalate, traceable to SRM from NIST and PTB pH 4.01 (25°C) Certipur®	Merck
Calcium chloride	Anhydrous free-flowing Redi-Dri™ ≥97%	Sigma-Aldrich
Calcium hydroxide		
Dipotassium phosphate	Analytical grade	Sigma-Aldrich
Hydrochloric acid	30% Suprapur®	Merck
Magnesium phosphate	Tribasic hydrate 98+%, pure	Thermo Scientific
Nitric acid	65% AnalaR NORMAPUR® analytical reagent	VWR Chemicals
Phosphoric acid	99%	Sigma-Aldrich
Sodium hydroxide	Baker analyzed	J.T. Baker™
Sodium molybdate(VI) dihydrate	99+%	Thermo Fisher Scientific
tri-Calcium phosphate	GPR RECTAPUR	VWR Chemicals
Ultrapure Water	18.2 Mohm	Veolia

5.2 Experimental procedure

5.2.1 Hydroxyapatite syntheses

Hydroxyapatite can precipitate in solutions including calcium and phosphorus in certain conditions. Two syntheses were prepared to create hydroxyapatite. Subsequently, the leaching behaviour of hydroxyapatite was compared with leaching behaviour of Ca-phosphate and Ca-P containing ashes.

Firstly, a wet chemical precipitation following the procedure outlined by Yelten-Yilmaz and Yilmaz,[47] was prepared, with some modifications to suit the experiment. In the first step, a $Ca(OH)_2$ suspension and H_3PO_4 solution were prepared. For the suspension, 12.24 g of $Ca(OH)_2$ (≥97%) was added to 75 mL water to obtain a 2.2 M solution. The phosphoric acid solution was prepared by weighing 8.18 g of H_3PO_4 (99%) and dissolving it in 75 mL of water. When both solutions were prepared the H_3PO_4 solution was added dropwise to the $Ca(OH)_2$ suspension, which created a precipitate that was left overnight to gain a stable state. The wet precipitate was dried at 110 °C for 7 hours and then cooled to room temperature. The semi-dry precipitate was heat-treated at 1250 °C for 2 hours. The cooling was then performed, with the first 30 minutes cooling to 800 °C. After cooling to 500 °C, the oven was shut off and left to cool by itself to room temperature.

The second hydroxyapatite synthesis followed the procedures outlined by Zhang et al[48] using a hydrothermal synthesis to prepare hydroxyapatite. The final steps of the synthesis were removed from the experimental protocol since it was determined that the precise morphology was not important for this experiment. Unlike the preceding synthesis, this synthesis method incorporates calcium chloride and phosphoric acid solutions, utilizing a controlled pH environment. For the calcium solution, 3.33 g of $CaCl_2$ was added in 20 mL of water and stirred for 15 minutes at room temperature. The phosphoric acid solution was prepared by weighing 2.07 g of H_3PO_4 (99%), dissolving it in 20 mL of water, and stirring the mixture for 15 minutes at room temperature. Afterwards, 6 M NaOH was added to the phosphate solution to adjust the pH to 10 and stirred for 30 minutes at room temperature. Then the calcium solution was slowly added to the phosphate solution, which gave a white precipitate. Two

preparations were prepared, differing in the ageing process of the white precipitate. One sample was aged overnight in a 100 °C oven with the lid on but not sealed, while the other had the lid sealed. Afterwards, about 20 mL of water was added to the precipitate solution and then filtered using Whatman Grade 40 Ashless Filter Paper with a diameter of 90 mm and a pore size of 8 µm.

5.2.2 Leaching of phosphate compounds

Three different phosphates, $AlPO_4$, $Ca_3(PO_4)_2$, and $Mg_3(PO_4)_2$, were investigated to see their behaviour and solubility in water. For each phosphate, 500 mg was added to 100 mL of pure water, and the mixture was stirred for 30 minutes in a closed-lid flask. After mixing, 1 mL of each sample was diluted with water to 100 mL and 1000 mL, respectively. For quantification of the dissolved phosphates, 10 mL of each sample was measured, and 2 mL of the reagent mixture was added to the diluted sample (see section *5.2.4 Molybdenum blue procedure*). After 15 minutes, if the colour appeared too dark, it indicated that the concentration exceeded the optimal range for accurate detection by UV-Vis. In such cases, further dilution of the sample was necessary to bring it within the calibration range. The ratios tested for $Ca_3(PO_4)_2$ were 1:50, 1:100, and 1:1000; for $AlPO_4$ ratios of 1:10, 1:50, and 1:100; and $Mg_3(PO_4)_2$ ratios of 1:100, 1:250, and 1:1000. The 1:1000 for $Mg_3(PO_4)_2$ and the 1:100 ratios for $AlPO_4$ and $Ca_3(PO_4)_2$ were tested after 3 hours of mixing to see if there were changes in the concentration. The pH for these ratios was around pH 9 or pH 5.5 for $AlPO_4$. Additionally, samples with pH around 2 and 4 were tested to discover how a lower pH affects the solubility of the phosphates. For the pH 4 samples, 500 mg of phosphates was mixed with 30 mL of Certipur® Buffer Solution pH 4 and water in a closed-lid flask, resulting in a total volume of 100 mL. After 30 minutes of mixing, 1 mL of each sample was diluted with water to a total volume of 50 mL for $AlPO_4$ and $Ca_3(PO_4)_2$, and 250 mL for $Mg_3(PO_4)_2$. For the test at pH 2, 500 mg of phosphate was added with 100 mL of 0.1 M HCl. In the case of $Mg_3(PO_4)_2$, additional $Mg_3(PO_4)_2$ was added as the first 500 mg seemed to have dissolved almost completely during the start of mixing. With the first 500 mg of $Mg_3(PO_4)_2$, a few drops of 30% HCl were added at the beginning of mixing to lower the pH to 2, but the pH became higher when the additional 500 mg was added into the mixture, which was left at pH 5.8. After 30

minutes of mixing, dilution factor of 1:1000 with 0.1 M HCl was prepared for $AlPO_4$ and $Ca_3(PO_4)_2$, and 1:10000 for $Mg_3(PO_4)_2$. The samples were then analyzed with a UV-Vis spectrophotometer.

A parallel experiment was conducted using 500 mg of each phosphate ($AlPO_4$, $Ca_3(PO_4)_2$, and $Mg_3(PO_4)_2$), which was added to 50 mL of either 0.1 M or 1 M HCl. The pH was measured during the mixing to assess if the pH needed to be adjusted. The mixtures were mixed for at least 2 hours before samples were diluted and analyzed with a UV-Vis spectrophotometer.

Finally, a mixture of two different phosphates was examined on their leaching behaviour. For the phosphate mixtures 250 mg of one of the three phosphates, $AlPO_4$, $Ca_3(PO_4)_2$, or $Mg_3(PO_4)_2$, and then 250 mg of another of the three phosphates were mixed. This created 3 samples: $AlPO_4 + Ca_3(PO_4)_2$, $AlPO_4 + Mg_3(PO_4)_2$, or $Ca_3(PO_4)_2 + Mg_3(PO_4)_2$. A total of six samples were prepared where the total amount of 500 mg phosphates was added to 50 mL 0.1 M or 1 M HCl. The mixtures were mixed for at least 2 hours before samples were diluted and analyzed with a UV-Vis spectrophotometer. In Table 3, the different phosphate samples are listed along with their corresponding solvents, dilution factors, and mixing times.

Table 3. List of single and mixed phosphate samples at room temperature. Note: 'Al,' 'Mg,' and 'Ca' represent $AlPO_4$, $Mg_3(PO_2)_4$, and $Ca_3(PO_2)_4$, respectively.

Sample name	Solvent	Dilution factor	Mixng time (hours)
Al 1:10 H_2O	H_2O	10	0.5
Al 1:100 H_2O	H_2O	100	0.5
Al 1:100 H_2O 3h	H_2O	100	3
Al 1:50 H_2O	H_2O	50	2
Al 1:50 pH 4	H_2O + buffer solution	50	2
Al 1:1000 0.M HCl	HCl	1000	2
Al 1:1000 0.1 M HCl	HCl	1000	2
Al 1:5000 0.1 M HCl	HCl	5000	2
Al 1:10000 0.1 M HCl	HCl	10000	2
Ca 1:1000 H_2O	H_2O	1000	0.5
Ca 1:100 H_2O	H_2O	100	0.5
Ca 1:100 H_2O 3h	H_2O	100	3
Ca 1:50 H_2O	H_2O	50	2
Ca 1:50 pH 4	H_2O + buffer solution	50	2
Ca 1:1000 0.1 M HCl	HCl	1000	2
Ca 1:1000 0.1 M HCl	HCl	1000	2
Mg 1:100 H_2O	H_2O	100	0.5
Mg 1:1000 H_2O	H_2O	1000	0.5
Mg 1:1000 H_2O 3h	H_2O	1000	3
Mg 1:250 H_2O	H_2O	250	2
Mg 1:250 pH 4	H_2O + buffer solution	250	2
Mg 1:5000 0.1 M HCl	HCl	5000	2
Mg 1:10000 0.1 M HCl	HCl	10000	2
Al+Ca 1:10 H_2O	H_2O	10	2
Al+Ca 1:50 H_2O	H_2O	50	2
Al+Mg 1:50 H_2O	H_2O	50	2
Al+Mg 1:100 H_2O	H_2O	100	2
Ca+Mg 1:100 H_2O	H_2O	100	2
Al+Ca 1:500 0.1 M HCl	HCl	500	2
Al+Ca 1:1000 0.1 M HCl	HCl	1000	2
Al+Mg 1:1000 0.1 M HCl	HCl	1000	2
Ca+Mg 1:1000 0.1 M HCl	HCl	1000	2
Al+Ca 1:500 1 M HCl	HCl	500	2
Al+Ca 1:1000 1 M HCl	HCl	1000	2
Al+Mg 1:1000 1 M HCl	HCl	1000	2
Ca+Mg 1:1000 1 M HCl	HCl	1000	2

5.2.3 Leaching of phosphorus from biomass ash

Ashes produced from rapeseed cake (RSC), wheat bran (WB) and sunflower seed shells (SSS) were used to investigate the leaching of phosphorus from various biomass ashes. The ash was produced by combusting pellets of the various fuel samples in an electrically heated furnace in 800 °C for around 24 hours. Then, approximately 500 mg of each biomass ash was added to a closed-lid flask filled with 50 mL water and stirred for 2 hours. The pH was measured at the beginning and again after 2 hours of mixing. After mixing, the samples were filtered using Whatman Grade 40 Ashless Filter Paper with a diameter of 90 mm and a pore size of 8 µm. Then, 10 mL of each leachate was taken and mixed with the MB reagent mixture for the quantification of dissolved phosphorus (see section *5.2.4 Molybdenum blue procedure*). After 15 minutes, if the colour appeared too dark, it indicated that the concentration exceeded the optimal range for accurate detection by UV-Vis. In such cases, further dilution of the sample was necessary to bring it within the calibration range. From both RSC and SSS, 2 mL was taken and then filled with water to 20 mL which gives a dilution factor of 1:10.

Further experiments were performed at lower pH around pH 1-2. These were conducted with two different acids: 0.1 M HNO_3 and 0.1 M HCl. The two acids were chosen to assess whether the leaching process was influenced by oxidizing acids or pH variations. The quantity of biomass ash added to the various acids varies, as the undissolved ash collected on the filter from water leaching is used. This was because of the limited supply of biomass ash available for use. The ash from each of the three substances (RSC, WB, and SSS) was divided into two equal parts. One part of each substance was mixed with 50 mL of 0.1 M HCl, while the other part was mixed with 50 mL of 0.1 M HNO_3. This process was carried out for each of the substances (RSC, WB, and SSS). It was then mixed for 2 hours in a closed-lid flask. Then, 10 mL of each sample was measured, and 2 mL of the reagent mixture was added (see section *5.2.4 Molybdenum blue procedure*). After 15 minutes, depending on the colour change, some ratio adjustments were made. Both a ratio of 1:10 and 1:100 was conducted on RSC and SSS with the different acid mixtures, but the visible colour change was only slight with RSC. Therefore, the RSC samples with HCl or HNO_3 were diluted to ratios of 1:1000. The samples were then analyzed with a UV-Vis spectrophotometer.

5.2.4 Molybdenum blue procedure

The method follows the procedure from DGT research.[49] The reagents used are 2.5 M H_2SO_4, 40 g/L of sodium molybdate (Na_2MoO_4), 2.8 mg/L of potassium antimony tartrate ($K_2Sb_2(C_4H_2O_6)_2$), and 17.6 g/L ascorbic acid ($C_6H_8O_6$). These are prepared by mixing 136 mL of H_2SO_4 to 1000 mL with water, 20 g of sodium molybdate into 500 mL of water, 0.28 g of sodium antimony tartrate into 100 mL water, and 1.76 g of ascorbic acid into 100 mL of water. A reagent mixture of 20 mL is prepared by adding 10 mL H_2SO_4, 3 mL sodium molybdate, 1 mL sodium antimony tartrate, and 6 mL ascorbic acid together. Then, 2 mL of the reagent mixture is added to 10 mL of the sample. Instead of adding 1 mL reagent mixture and 5 mL sample, as the procedure from DGT research, a higher amount is prepared for cleaning the cuvette in the UV-Vis spectrophotometer.

5.2.5 Quantification of phosphates

Standard solutions with known concentrations ranging from 1 to 10 ppm were used to create a calibration line which was used for the quantification of phosphates in the solution samples from the experiments. The standard solutions were prepared by adding 1.73 mg of K_2HPO_4 into 1 L of water to obtain 100 ppm, which was then diluted further to 1 ppm, 2 ppm, and so forth to 10 ppm. Additionally, chloride was added to samples containing 2 or 5 ppm phosphate and compared to the pure standard solutions to clarify whether chloride will affect the analysis method. Specifically, 5 mL of each concentration was combined with different mixtures: 5 mL H_2O, 1 mL diluted HCl and 4 mL H_2O, or 5 mL diluted HCl. Then 10 mL was taken from all 16 samples, and each was mixed with 2 mL of the MB mixture. Also, a blank was created with 10 mL of water and then 2 mL of the MB mixture. After at least a 15-minute wait, the samples were measured with a UV-Vis spectrophotometer to gain an understanding of when the concentration in each sample was too high to be measured correctly. The range of wavelength measured with UV-Vis spectrophotometer was between 190 and 900 nm to detect if anomalies were seen. Preparing a sample for measurements follows the same procedure as preparing standard solutions, involving the addition of 2 mL MB mixture to 10 mL of the sample and allowing it to sit for at least 15 minutes. The

cuvette is cleaned with ethanol and then water before and after use. To obtain an accurate measurement the cuvette is rinsed with the sample first and then ¾ of the cuvette is filled with the sample for measuring. Between each measurement, the cuvette is only rinsed with the sample to be measured.

6 Results and Discussion

6.1 Construction of the calibration curve

The spectrograms from the UV-VIS measurements with the standard solutions are shown in Figure 8. The absorbance at the characteristic peak at 710 nm was plotted against the concentration to obtain the calibration line. The peak at 710 nm was analyzed following the MB method with ascorbic acid and Sb(III).[37] The peak values were not consistently observed strictly at 710 nm; instead, they were situated within the 700 to 720 nm range. Nonetheless, the values were taken at 710 nm for consistency. Beyond the 8 ppm concentration, the peak at 710 nm lost distinctiveness, suggesting that the detection limit had been surpassed.

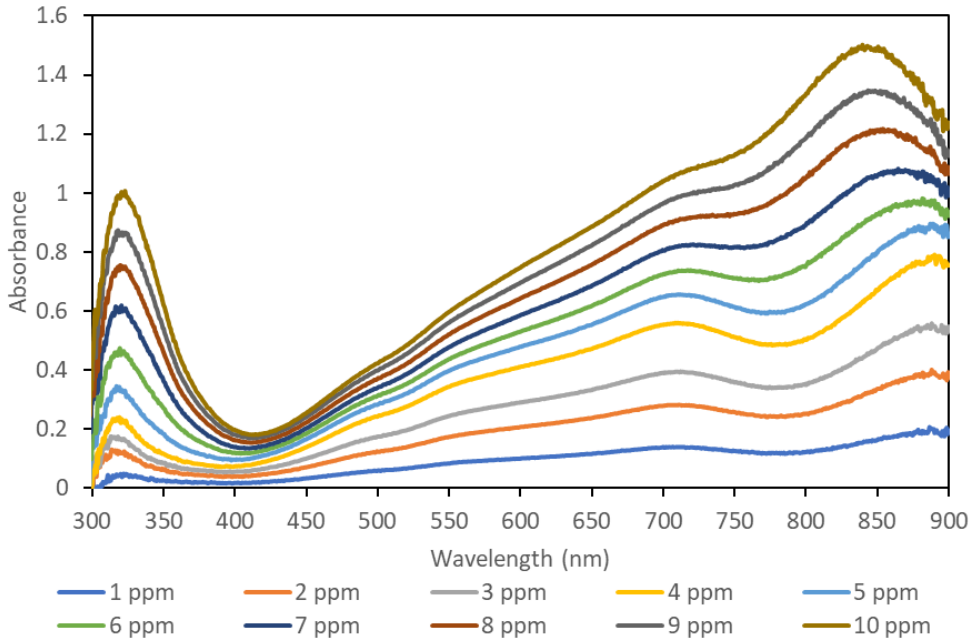

Figure 8. UV-Vis spectra of a standard solution of phosphorus with known concentrations between 1 and 10 ppm.

The Beer-Lambert law states that the concentration of the substance is directly proportional to its absorbance.[34] This relationship is used to construct a calibration curve, plotting absorbance at 710 nm against concentration from the spectra (Figure 9).[35] Due to the spectrophotometer's detection limit, the reliability of the calibration curve diminishes as concentrations move beyond a certain threshold, at which point the data deviates from the linear trend. A calibration curve was initially constructed

within the range of 1 to 10 ppm. However, because of the peak distinctiveness plateauing after 8 ppm (Figure 8), a calibration curve was established within the range of 1 to 7 ppm as it does not follow the Lambert-Beer law after 8 ppm. The absorbance at 4 ppm is considered as a potential outlier due to the observed plateauing in Figure 8. Consequently, the linear trend observed between 1 to 4 ppm is considered unreliable due to the influence of this outlier and is excluded from the analysis as a potential linear trend (Figure 9). The detection limit was set at 1 ppm, as the values below were not measured. This showed that the absorbance for the peak at 710 nm should be between 0.1 and 1. Therefore, when the UV-VIS spectrophotometer is used for the determination of a sample concentration, solutions between 1 and 7 ppm were used to create calibration curves for each run. The colour change observed for the visible eye in 1 to 7 ppm, was used as references when sample dilutions were made before analyzing with a UV-Vis spectrophotometer (Figure 10).

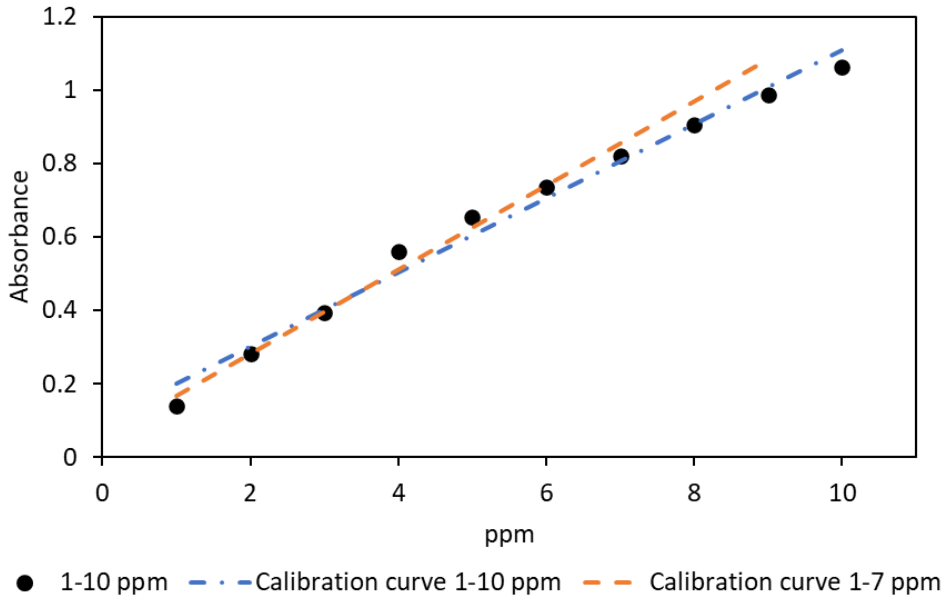

Figure 9. Calibration curve of absorbance at 710 nm against concentrations of standard solutions between 1 to 10 ppm.

Figure 10. Phosphate concentration in samples 1 to 10. Sample 1 exhibits a phosphate concentration of 1 ppm, and as the concentration increases in subsequent samples (2 to 10), the blue colour intensifies. The blue colour is due to the added reagent mixture from the molybdenum blue method. The blank (clear) sample is water with the reagent mixture.

Table 4 shows variations in the absorbance with different chloride concentrations due to the addition of diluted HCl. At 2 ppm, a slight decrease is observed with added chloride, while at 5 ppm, a minor increase is noted. These changes are subtle, and further investigation with higher concentrations is required for a more comprehensive understanding.

Table 4. Absorbance at 710 nm of standard solution 2 and 5 ppm combined with diluted HCl (~0.1 M) to inspect the effect of chloride, obtained with UV-Vis spectrophotometer

Sample	Absorbance
5 mL 2 ppm + 5 mL H_2O	0.142
5 mL 2 ppm + 4 mL H_2O + 1 mL HCl	0.142
5 mL 2 ppm + 5 mL HCl	0.136
5 mL 5 ppm + 5 mL H_2O	0.351
5 mL 5 ppm + 4 mL H_2O + 1 mL HCl	0.352
5 ppm 5 mL HCl	0.353

6.2 Determination of phosphorus concentration

6.2.1 Leaching behaviour of single phosphate compounds

As seen in section 6.1 phosphate concentrations need to be below 7 ppm for accurate quantification. Hence, the samples from the leaching tests were diluted at different ratios to find the conditions at which the phosphate concentration could be quantified. Table 5 lists the dilutions of all the individual phosphate mixtures in water, pH 4, or HCl below. The dilution factors are expressed as 1:50, which means that a sample of 1 mL was diluted to 50 mL with water, pH 4, or HCl depending on the solute of the sample. The dilutions depended on the colour change from the molybdenum blue method. If a colour darker than 7 ppm was observed, the samples were diluted until the colour was between 1 to 7 ppm. The samples leached in 1 M HCl did not change colour and therefore they have not been analyzed with a UV-Vis spectrophotometer. This might be due to it being too acidic for PMB species to form. Firstly, the dilution factor is higher in the samples leached in HCl compared to water, which already indicates a higher concentration of phosphorus. Secondly, the dilution factor between the different phosphate compounds is different in the same solvents. Higher dilution for $Mg_3(PO_4)_2$ was needed, as more Phosphorus was leached.

Table 5. Dilution factors of different phosphorus compounds in water, pH 4 or 0.1 M HCl

	$AlPO_4$	$Ca_3(PO_4)_2$	$Mg_3(PO_4)_2$
H_20	1:50	1:50	1:100
	1:100	1:100	1:250
			1:1000
pH 4		1:50	1:250
HCl	1:1000*	1:1000**	1:5000**
	1:5000*		1:10000
	1:10000		

*Only 500 mg in 50 mL HCl samples were diluted **Both 500 mg in 50 and 100 mL in HCl samples were diluted.

These dilution samples were tested with the UV-Vis spectrophotometer and in Figure 11 the spectra for $Ca_3(PO_4)_2$ samples are shown, and the spectra for $AlPO_4$ and

$Mg_3(PO_4)_2$ samples are in Appendix A. The spectra show that samples with HCl, pH 4 buffer, or water can be measured.

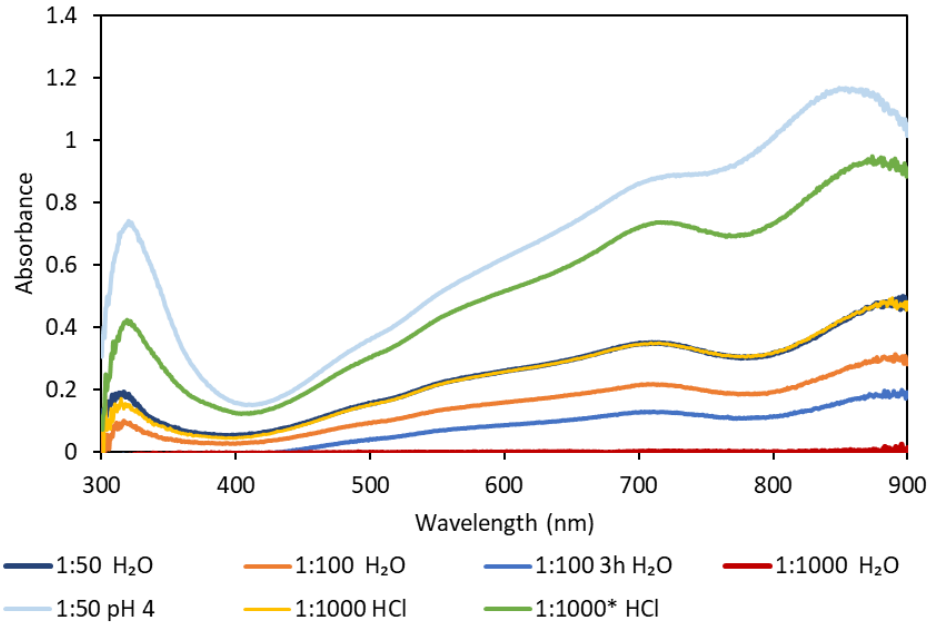

Figure 11. UV-Vis spectra of $Ca_3(PO_4)_2$ samples in water, pH 4 and HCl in different dilutions. Sample 1:1000 HCl (yellow) is on top of sample 1:50 pH 4 (dark blue) and therefore difficult to see.

The concentration of leached phosphorus was calculated from the absorbance value at the peak of 710 nm using the calibration curve. The next step was to calculate the dilution of the samples; both from the mixed reagent and the dilution in Table 5. After determining the phosphate concentrations following the dilution adjustments, the phosphorus content was subsequently calculated from these phosphate concentrations. All the calculations and steps can be found in Appendix B. The phosphorus concentrations, measured in mmol/L for 500 mg in 100 mL solvent, are presented in Table 6. It is observed that for the same phosphate compound samples leached in water display similar phosphorus concentrations. For example, $AlPO_4$ 1:100 and $AlPO_4$ 1:100 3h are the same sample, but the former is measured at 30 minutes of mixing and the latter at 3 hours of mixing. This difference may account for the lower concentration, even though the leaching parameters should be the same. For $Ca_3(PO_4)_2$ leached in water, the lower concentration of $Ca_3(PO_4)_2$ 1:100 3h compared to $Ca_3(PO_4)_2$ 1:100 might be due to the formation of hydroxyapatite. If mixing continued, the amount of phosphate ions in the solvent would diminish, as hydroxyapatite would

precipitate. Moreover, the concentration of phosphorus increases in samples in pH 4 buffer solution compared to those in water, and it is even higher in samples leached in HCl. The $AlPO_4$ 1:10000 in 0.1 M HCl might be inaccurate, as the recorded value is exceptionally high. A cross-reference with measurements in Appendix B, specifically Al 1:1000 0.1 M, which adopted a lower dilution of 1:1000, reveals results below the detection limits. This discrepancy suggests a potential anomaly or error in the 1:10000 dilution data.

Table 6. Phosphorus concentration after leaching 500 mg of phosphate compounds in 100 mL of solvent for 30 min or 3 h obtained with UV-Vis spectrophotometer

Solvent	Sample and dilution	mmol/L
	$AlPO_4$ 1:100	1.3
H_2O	$AlPO_4$ 1:100 3h	1.4
	$AlPO_4$ 1:50	0.7
0.1 M HCl	$AlPO_4$ 1:10000	103
	$Ca_3(PO_4)_2$ 1:100	2.0
H_2O	$Ca_3(PO_4)_2$ 1:100 3h	1.2
	$Ca_3(PO_4)_2$ 1:50	1.6
pH 4	$Ca_3(PO_4)_2$ 1:50 pH 4	4.2
0.1 M HCl	$Ca_3(PO_4)_2$ 1:1000	33
	$Mg_3(PO_4)_2$ 1:1000	9.6
H_2O	$Mg_3(PO_4)_2$ 1:250	5.8
	$Mg_3(PO_4)_2$ 1:100	7.3
pH 4	$Mg_3(PO_4)_2$ 1:250 pH 4	19
0.1 M HCl	$Mg_3(PO_4)_2$ 1:10000	186

The phosphorus concentrations, measured in mmol/L for 500 mg in 50 mL solvent, are presented in Table 7. Phosphorus concentration in the solution increased in the

following order: $AlPO_4<Ca_3(PO_4)_2<Mg_3(PO_4)_2$. The trend could also be seen with most of the samples in Table 6.

Table 7. Phosphorus concentration of leaching 500 mg of phosphate compounds in 50 mL of 0.1 M HCl obtained with UV-Vis spectrophotometer mixed for 2 hours

Sample and dilution	mmol/L
$AlPO_4$ 1:1000	3.6
$Ca_3(PO_4)_2$ 1:1000	9.3
$Mg_3(PO_4)_2$ 1:5000	9.9

The solubility of $AlPO_4$, $Ca_3(PO_4)_2$, and $Mg_3(PO_4)_2$ in water was either non soluble, had no data, or the data was inconsistent, making it challenging to predict the extent of solubility, if any. Table 6 and Table 7 present the order of solubility derived from the experiments conducted in both water, buffer solution, and 0.1 M HCl, from the least soluble to the most soluble: $AlPO_4 < Ca_3(PO_4)_2 < Mg_3(PO_4)_2$. It is worth noting that this conclusion considers the observed anomaly in $AlPO_4$ 1:1000 0.1 M HCl. This anomaly is acknowledged and therefore excluded from the established order of solubility. The reason for this order can be explained by the hard and soft acids and bases (HSAB) concept. HSAB is a concept introduced by Pearson[50] which states that "hard acids prefer to coordinate to hard bases and soft acids to soft bases". The acids and bases can be categorised into hard, soft, and borderline. Hard acids or bases are categorized with the following qualities: small radius, low polarizability, high oxidation state and electronegativity. Soft acids and bases are categorized with the following qualities: large radius, high polarizability, low oxidation state and electronegativity. The borderline (also known as intermediate) acids and bases are between being hard and soft. Aluminium, calcium, and magnesium are categorized as hard acids and PO_4^{3-} is considered a hard base. Aluminium exhibits an oxidation state of III, while calcium and magnesium have an oxidation state of II. The atomic radius follows an increasing order, starting with the smallest radius for aluminium, followed by magnesium, and then calcium. Also, aluminium possesses the highest electronegativity, followed by magnesium and calcium. All of this explains why $AlPO_4$ is less soluble than $Ca_3(PO_4)_2$ and $Mg_3(PO_4)_2$ as PO_4^{3-} has a stronger ionic bond with Al^{3+} than Mg^{2+} and Ca^{2+}.

This section presents the investigation into the behaviour of phosphorus compounds under varying pH conditions. FactSage was employed to analyze the equilibrium and leaching behaviours of these compounds across a range of pH values. In Figure 12, the total amount of phosphorus leached from $AlPO_4$ is presented. The values obtained from FactSage calculations are represented in grey, while the values obtained from the experiments conducted for this thesis are in orange. The orange values had higher phosphorus concentrations than the equilibrium values at the same pH. This may be due to the dilution process, where small errors become more pronounced as concentrations decrease. Hence, it could explain why the experimental points differ from the calculated equilibrium values. The margin of error for pH measurements was 0.2, while for the concentration, it was 10%. Calculating the exact error is challenging due to the multiple steps in the process that could impact measurements, such as errors in temperature during UV-Vis, as well as in volume and mass measurements. The red dashed line represents the maximum amount of phosphorus that can be leached from 500 mg of $AlPO_4$. For example, the closest experimental value to the total phosphorus concentration exhibits a concentration difference of approximately 35 mmol/L, equating to 11% of the total phosphorus being leached.

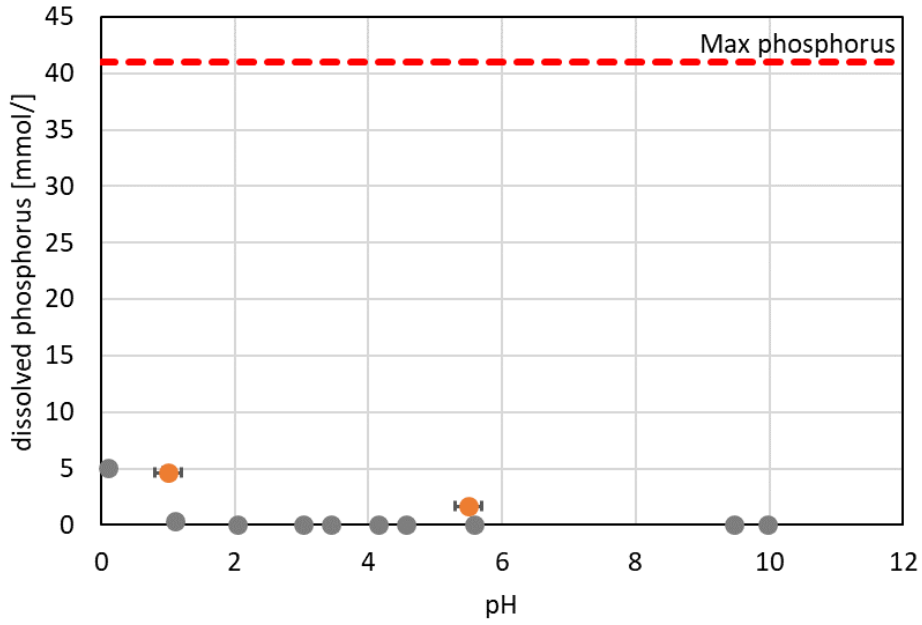

Figure 12. Equilibrium calculations of $AlPO_4$ across a range of pH values, with FactSage equilibrium calculations displayed in grey and experimental data in orange. The red dashed line represents the maximum amount of phosphorus that can be leached from 500 mg of $AlPO_4$.

In Figure 13 and Figure 14, the total amount of phosphorus leached from $Ca_3(PO_4)_2$ is presented. The difference is that in Figure 13 the formation of hydroxyapatite has been taken into consideration in the calculations, whereas in Figure 14 it has not been taken into consideration. The experimental values are closer to the equilibrium values in the formation of hydroxyapatite than the one without. The total phosphorus concentration is illustrated by a red dashed line. For example, the closest experimental value to the total phosphorus concentration exhibits a concentration difference of approximately 23 mmol/L, equating to 28% of the total phosphorus being leached.

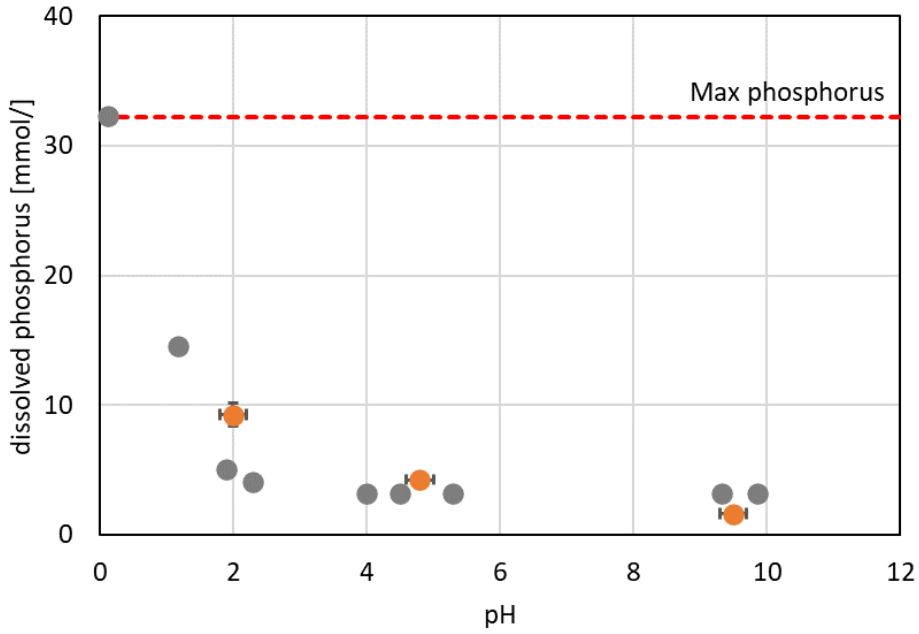

Figure 13. Equilibrium calculations of $Ca_3(PO_4)_2$ with hydroxyapatite across a range of pH values, with FactSage equilibrium calculations displayed in grey and experimental data in orange. The red dashed line represents the maximum amount of phosphorus that can be leached from 500 mg of $Ca_3(PO_4)_2$.

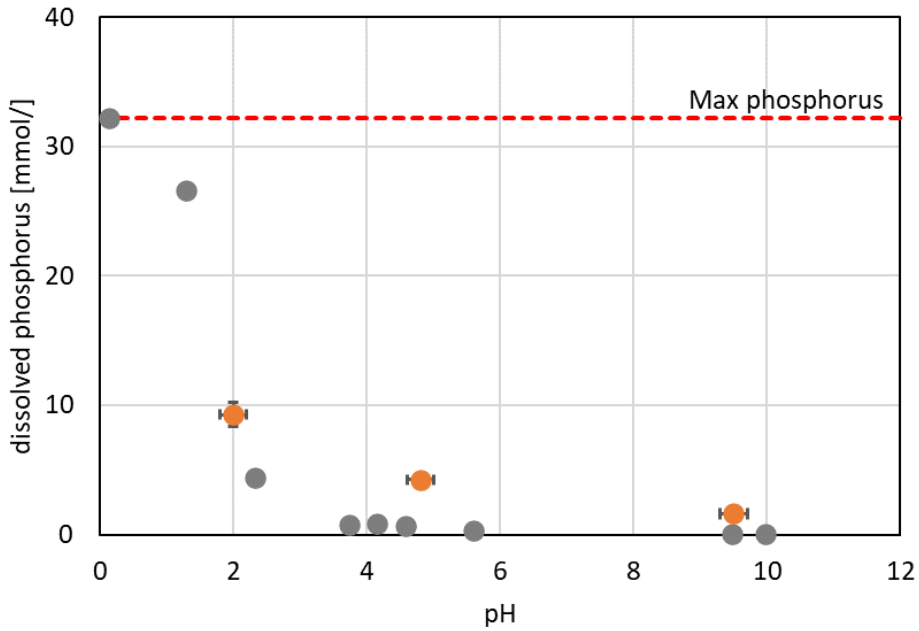

Figure 14. Equilibrium calculations of $Ca_3(PO_4)_2$ without hydroxyapatite across a range of pH values, with FactSage equilibrium calculations displayed in grey and experimental data in orange. The red dashed line represents the maximum amount of phosphorus that can be leached from 500 mg of $Ca_3(PO_4)_2$.

In Figure 15, the total amount of phosphorus leached from $Mg_3(PO_4)_2$ is presented. At pH 9 to 10, the equilibrium value is near zero, while the experimental value exhibits a notably higher concentration. Conversely, at pH 4, the orange value is only half of the equilibrium value. The total phosphorus concentration is illustrated by a red dashed line. For example, the experimental value to the total phosphorus concentration exhibits a concentration difference of approximately 19 mmol/L, equating to 49% of the total phosphorus being leached.

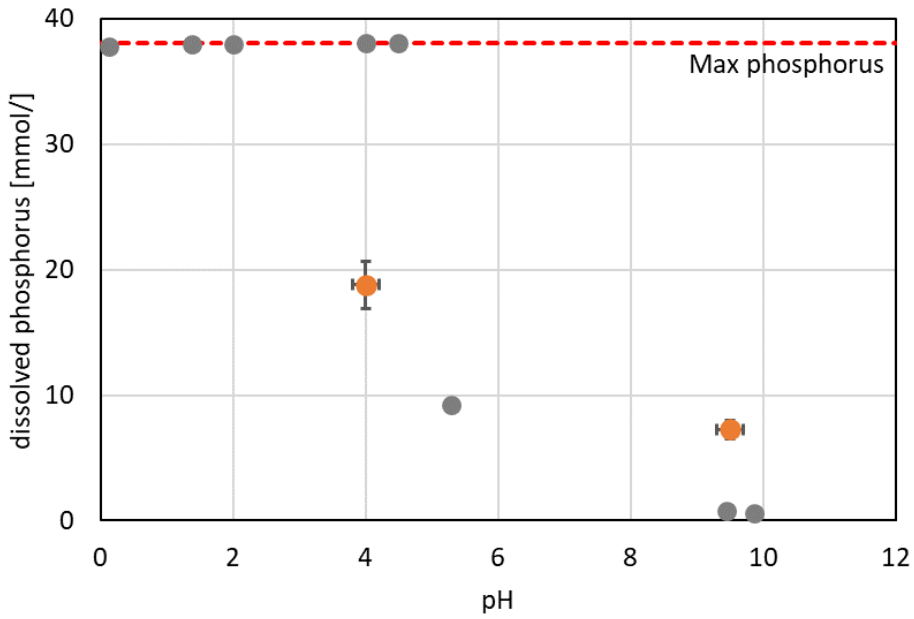

Figure 15. Equilibrium calculations of $Mg_3(PO_4)_2$ across a range of pH values, with FactSage equilibrium calculations displayed in grey and experimental data in orange. The red dashed line represents the maximum amount of phosphorus that can be leached from 500 mg of $Mg_3(PO_4)_2$.

In conclusion, the experiments of phosphate compounds provided insights into the leaching behaviour and solubility of phosphorus compounds under varying conditions. The results highlighted the influence of pH on leaching, with differences between experimental and equilibrium values. The observed differences were attributed to experimental factors, with a margin of error of 0.2 for pH measurements and 10% for concentration. The solubility trend, deduced from experiments, followed $AlPO_4$ < $Ca_3(PO_4)_2$ < $Mg_3(PO_4)_2$. The results were consistent with the hard and soft acids and bases concept.

6.2.2 Leaching behaviour of mixtures of two phosphate compounds

As the burning of biomasses is rarely composed of only one phosphate compound, mixtures of the phosphate compounds were tested. Both 0.1 M and 1 M HCl were mixed with the phosphates, but there was no colour change in the 1 M HCl samples during the molybdenum blue method. Therefore, for the UV-Vis measurement only water (Figure 16) and 0.1 M (Figure 17) samples were tested. Some phosphate

mixtures have two dilutions due to uncertainty in the required dilution factor, and on occasion, both dilutions fall within the calibration curve.

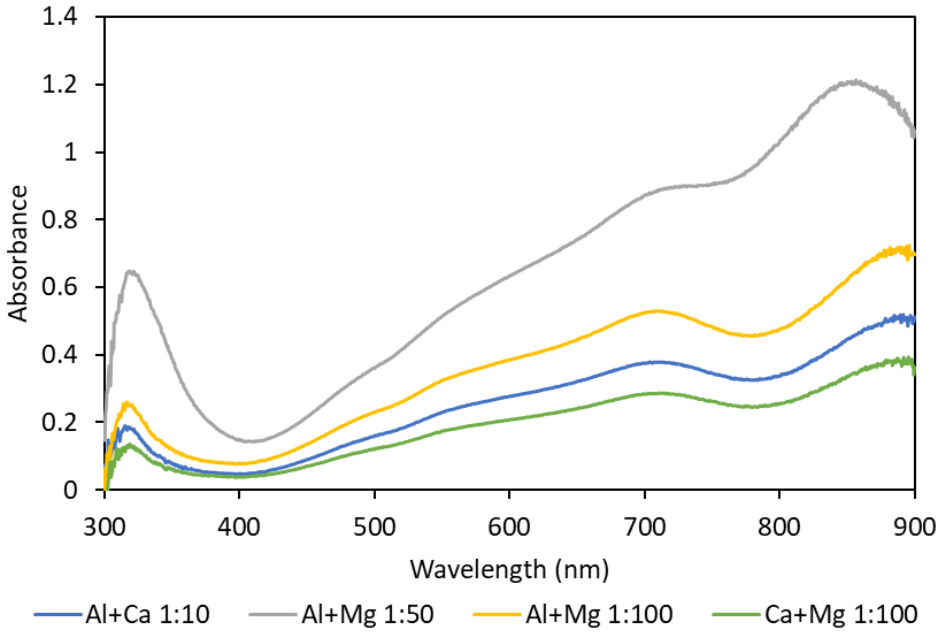

Figure 16. Phosphate compounds mixtures in water. Al is short for $AlPO_4$, Ca for $Ca_3(PO_4)_2$, and Mg for $Mg_3(PO_4)_2$.

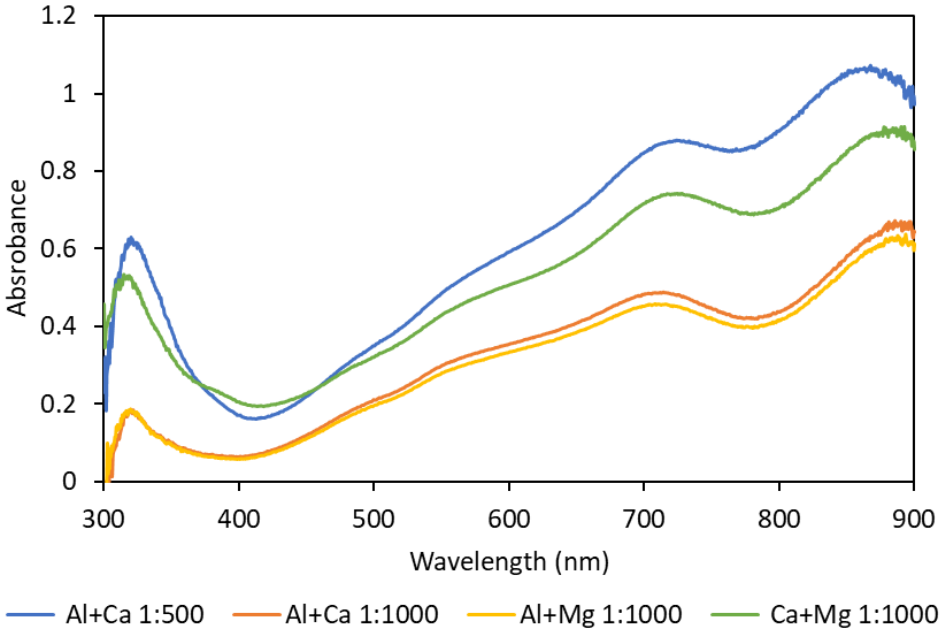

Figure 17. Phosphate compounds mixtures in 0.1 M HCl. Al is short for $AlPO_4$, Ca for $Ca_3(PO_4)_2$, and Mg for $Mg_3(PO_4)_2$.

In Table 8 the samples' phosphorus concentrations for leached phosphate mixtures in water or 0.1 M HCl are shown, and calculations can be found in Appendix B. The same samples, but with different dilutions can be seen to have similar concentrations, which indicates that an approximate concentration might be possible to obtain.

Table 8. Phosphorus concentration in leached phosphate mixtures obtained with UV-Vis spectrophotometer. Leaching of 500 mg phosphate compounds in 50 mL.

Solvent	Sample and dilution	mmol/L
H_2O	Al+Ca 1:10	0.35
	Al+Mg 1:50	4.12
	Al+Mg 1:100	4.92
	Ca+Mg 1:100	2.66
0.1 M HCl	Al+Ca 1:500	5.48
	Al+Ca 1:1000	6.14
	Al+Mg 1:1000	5.79
	Ca+Mg 1:1000	9.27

In Table 9, the concentrations of the leached samples with ICP-OES are presented, revealing values for aluminium, magnesium, calcium, and phosphorus. The values for phosphorus in ICP-OES were higher than the values from UV-Vis (Table 8) for the corresponding samples. This can be due to the molybdenum blue species not binding itself to the phosphate ion, as the phosphorus is still bound to other ions or has started to polymerize. The samples leached in 1 M HCl had a higher concentration of phosphorus than the samples leached in 0.1 M HCl. This is due to stronger acid concentration, which made it possible to leach more of the phosphorus.

Table 9. Concentrations of Al, Ca, Mg, and P in HCl-leached samples were analyzed with ICP-OES. The Al, Ca, and Mg in sample names refer to $AlPO_4$, $Ca_3(PO_4)_2$, and $Mg_3(PO_4)_2$.

Sample	Al (mmol/L)	Ca (mmol/L)	Mg (mmol/L)	P (mmol/L)
0.1 M HCl - Al+Ca	2.63	17.62	0.12	9.49
0.1 M HCl - Al+Mg	2.20	0.01	9.83	9.08
0.1 M HCl - Ca+Mg	0.01	15.78	9.47	11.75
1 M HCl - Al+Ca	6.13	17.69	0.10	11.77
1 M HCl - Al+Mg	4.23	0.01	8.49	10.11
1 M HCl - Ca+Mg	0.01	16.47	8.06	12.27

In Figure 18, equilibrium calculations of the total amount of phosphorus leached from a mixture of $AlPO_4$ and $Ca_3(PO_4)_2$ in a range of pH values. The calculations include the presence of hydroxyapatite. The values obtained from FactSage equilibrium calculations are represented in grey, yellow, and blue, while the values obtained from the experiments conducted for this thesis are in orange. The equilibrium phosphorus is the total phosphorus concentration of three phosphate ions: PO_4^{3-}, HPO_4^{2-}, and $H_2PO_4^-$. At a pH of 7.5, the experimental phosphorus concentration is lower than the values from the equilibrium calculations, whereas, at pH 2, it closely corresponds with the equilibrium value. Comparing the calculated amounts of leached phosphorus from $AlPO_4$ in Figure 12 with the total phosphorus leached depicted in Figure 18, a difference is observed. This difference could be attributed to the possibility that the solution was already saturated with phosphorus at pH 0, considering the low solubility of $AlPO_4$.

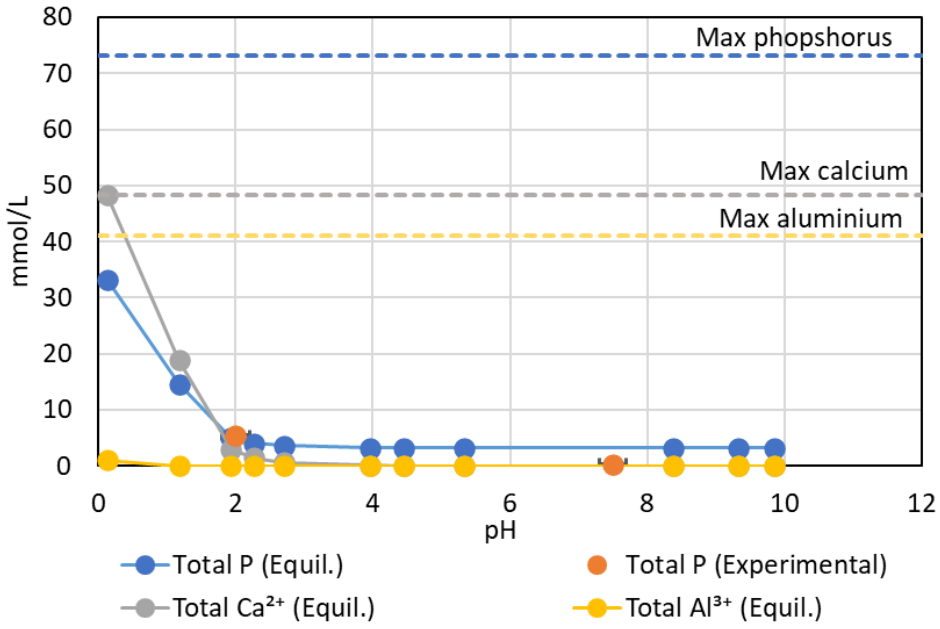

Figure 18. Equilibrium calculations of $AlPO_4$ and $Ca_3(PO_4)_2$, including the presence of hydroxyapatite, across a range of pH values. FactSage equilibrium calculations are displayed in blue, and experimental data in orange. Total calcium concentration from equilibrium calculations is represented in grey and aluminium in yellow. The corresponding colours, shown as dashed lines, highlight the maximum concentration that can be leached.

In Figure 19, equilibrium calculations of the total amount of phosphorus leached from a mixture of $AlPO_4$ and $Ca_3(PO_4)_2$ are presented, without the presence of hydroxyapatite included. The phosphorus concentration at pH 7.5 appears to be nearly zero in both the experimental and equilibrium data. At pH 2 the experimental value was around 5 mmol/L below the equilibrium phosphorus concentration. As discussed earlier (Figure 18), the trend of $AlPO_4$ exhibiting lower solubility in mixtures is also seen in these calculations. At pH 0, all $Ca_3(PO_4)_2$ should be dissolved according to the equilibrium calculations.

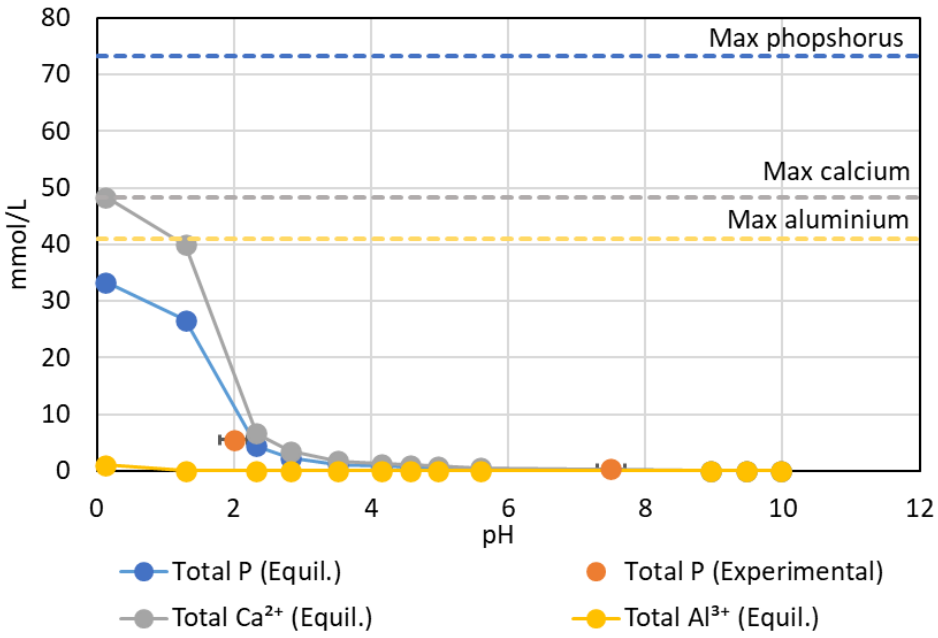

Figure 19. Equilibrium calculations of $AlPO_4$ and $Ca_3(PO_4)_2$ across a range of pH values, excluding the presence of hydroxyapatite. FactSage equilibrium calculations are displayed in blue, and experimental data in orange. Total calcium concentration from equilibrium calculations is represented in grey and aluminium in yellow. The corresponding colours, shown as dashed lines, highlight the maximum concentration that can be leached.

Figure 20 illustrates the equilibrium calculations for the total phosphorus leached from a mixture of $AlPO_4$ and $Mg_3(PO_4)_2$. The concentrations of phosphorus and magnesium reach a plateau at pH 5, and according to the equilibrium calculations all $Mg_3(PO_4)_2$ is dissolved, suggesting that the phosphorus originates from $Mg_3(PO_4)_2$. Conversely, at pH 2 and lower, there is a noticeable increase in phosphorus and aluminium concentrations, indicating the contribution of phosphorus from $AlPO_4$. Again, the trend of $AlPO_4$ exhibiting lower solubility in mixtures is also seen in these calculations.

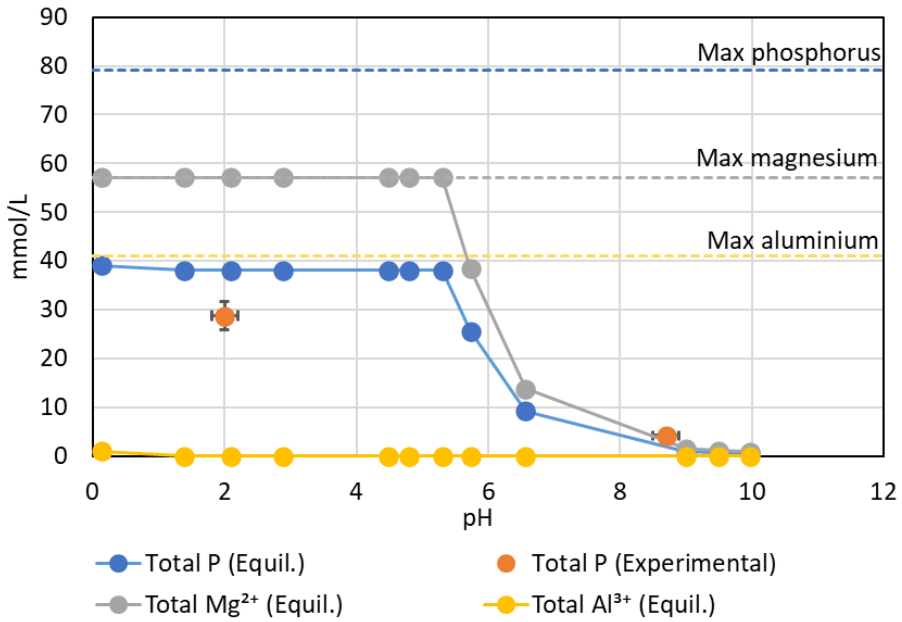

Figure 20. Equilibrium calculations of $AlPO_4$ and $Mg_3(PO_4)_2$ across a range of pH values. FactSage equilibrium calculations are displayed in blue, and experimental data in orange. Total magnesium concentration from equilibrium calculations is represented in grey and aluminium in yellow. The corresponding colours, shown as dashed lines, highlight the maximum concentration that can be leached.

Figure 21 provides an overview of equilibrium calculations depicting the overall phosphorus leaching from a mixture of $Ca_3(PO_4)_2$ and $Mg_3(PO_4)_2$, including the presence of hydroxyapatite. Here, a similar result of phosphorus and magnesium concentrations plateauing at pH 5, but the phosphorus concentration and calcium concentrations then rising after pH 3. The difference between the equilibrium and experimental concentrations at the same pH has a max difference of 6 mmol/L. In contrast to other phosphate mixtures where approximately half of the total phosphorus dissolves at pH 0, in this case, all phosphorus is expected to dissolve at pH 0. This can be attributed to no $AlPO_4$ being present.

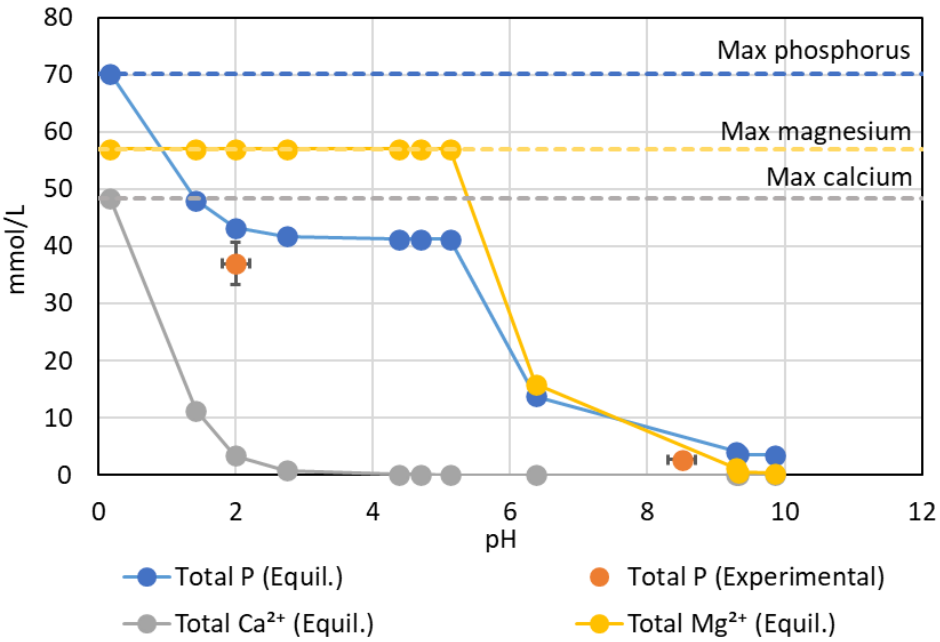

Figure 21. Equilibrium calculations of $Ca_3(PO_4)_2$ and $Mg_3(PO_4)_2$, including the presence of hydroxyapatite, across a range of pH values. FactSage equilibrium calculations are displayed in blue, and experimental data in orange. Total calcium concentration from equilibrium calculations is represented in grey and magnesium in yellow. The corresponding colours, shown as dashed lines, highlight the maximum concentration that can be leached.

In Figure 22, equilibrium calculations of the total amount of phosphorus leached from a mixture of $Ca_3(PO_4)_2$ and $Mg_3(PO_4)_2$ are presented, excluding the presence of hydroxyapatite. Again, the magnesium concentration plateaus after pH 5, with phosphorus rising with the magnesium first, and then with calcium at around pH 3. The difference between the equilibrium phosphorus and experimental phosphorus is 8.7 mmol/L. The same trend as seen in Figure 21, of all the phosphorus being dissolved at pH 0 can be seen.

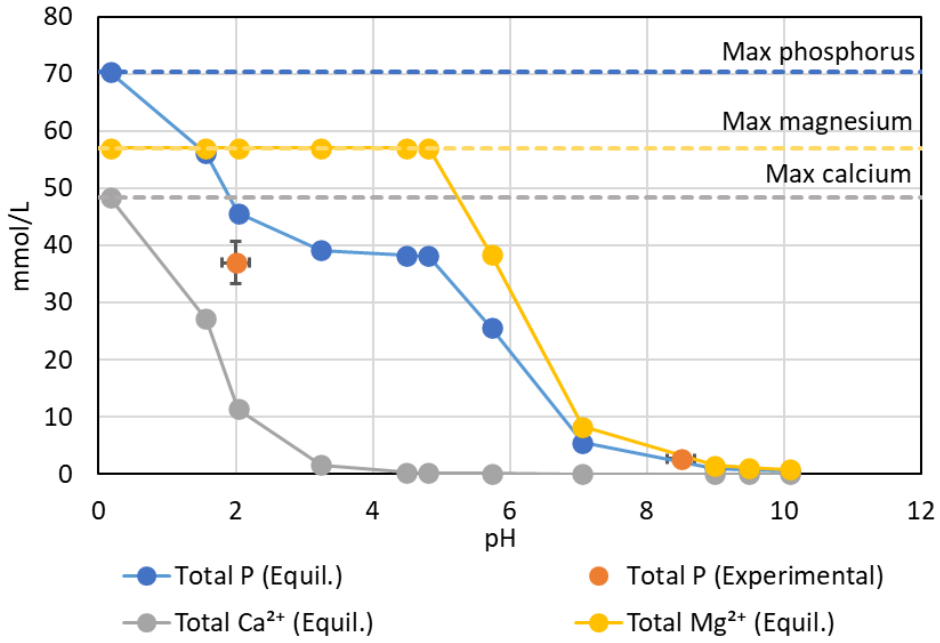

Figure 22. Equilibrium calculations of $Ca_3(PO_4)_2$ and $Mg_3(PO_4)_2$, excluding the presence of hydroxyapatite, across a range of pH values. FactSage equilibrium calculations are displayed in blue, and experimental data in orange. Total calcium concentration from equilibrium calculations is represented in grey and magnesium in yellow. The corresponding colours, shown as dashed lines, highlight the maximum concentration that can be leached.

In conclusion, the experiments on the leaching behaviour of phosphate mixtures provided valuable insights into their solubility under different conditions. The experiments, involving mixtures of phosphates with 0.1 M and 1 M HCl, highlighted the complex behaviour of these compounds. While 1 M HCl samples did not show colour change during the molybdenum blue method, those in water and 0.1 M HCl exhibited variations in phosphorus concentrations, as seen in Table 8. Also, in scenarios where $AlPO_4$ was not present, it was anticipated that all phosphorus should dissolve at pH 0. However, in scenarios where $AlPO_4$ was present, it was seen that less aluminium and phosphorus was dissolved in phosphate mixtures compared to leaching of $AlPO_4$ alone. This indicates that in more complex systems, less soluble phosphates will dissolve to a much lesser extent or may not dissolve at all. UV-Vis spectrophotometer analysis and ICP-OES results (Table 9) demonstrated differences in phosphorus concentrations, attributed to the limitations of the molybdenum blue method. Figure 18-Figure 22 studied the leaching behaviour, with or without taking the formation of hydroxyapatite into consideration for the equilibrium calculations. The experimental and equilibrium data showcased the interaction between different phosphate compounds with each other and pH. The experimental data and equilibrium

calculations were generally in good agreement. Deviations between experimental data and equilibrium calculations may be caused by uncertainties in the experimental results. Also, the time factor is not considered here, i.e. not all systems may be fully at equilibrium.

6.2.3 Leaching behaviour of hydroxyapatites

Analyses were carried out on the leaching behaviour of the apatites synthetized according to section 5.2.1. Noteworthy, is that the only difference in the synthesis of Apatite 2 and 3 was the lid in the oven, which was on and not sealed in Apatite 2, whereas in Apatite 3 it was sealed. This might be the cause of the different leaching behaviour of both Apatites. In Figure 23 the amount of phosphorus leached from the different apatites in different solvents is seen. In water (Figure 23a), all apatites showed relatively low dissolution compared to other solvents. At pH 4 (Figure 23b), Apatite 1 exhibited the highest dissolution of phosphorus, Apatite 2 dissolved one-fourth of that amount, and Apatite 3 exhibited minimal dissolution of 0.002 mmol/L. In both HCl and HNO_3 (Figure 23c and d) Apatite 3 showed zero phosphorus dissolution. Apatite 1 leached 20 mmol/L more phosphorus in HCl compared to HNO_3, while Apatite 2 had a 1 mmol/L difference between the two solvents.

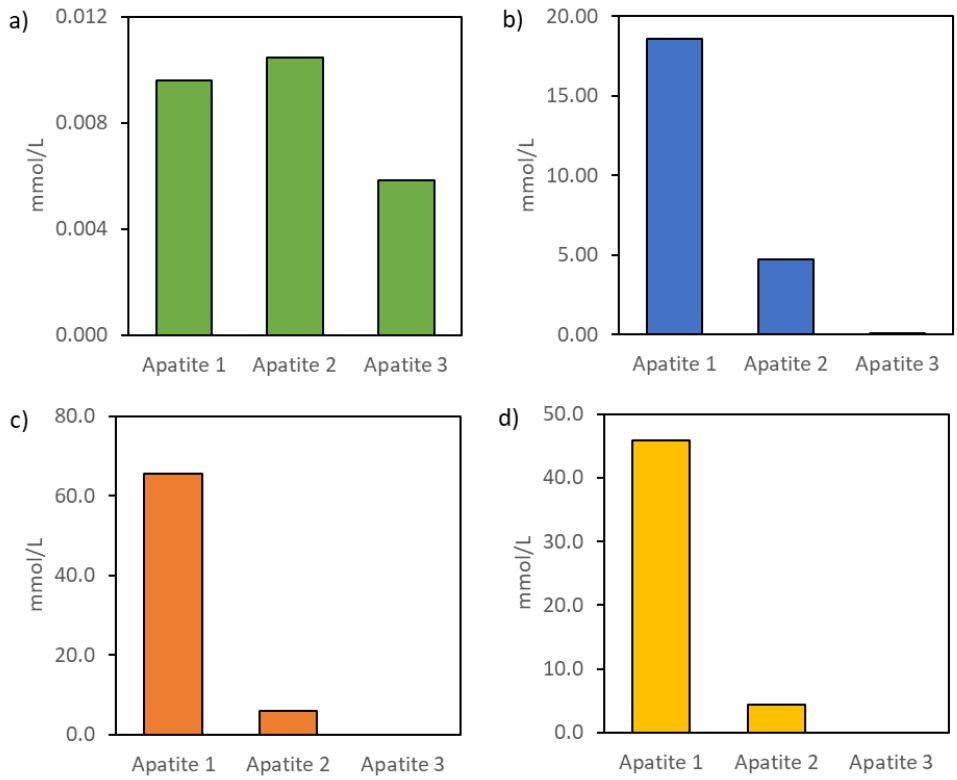

Figure 23. Apatites subjected to leaching in a) H_2O b) pH 4 c) HCl and d) HNO_3. Leaching was conducted with 500 mg of apatite in 50 mL. Apatite 1 is synthesized by chemical precipitation and apatite 2 and 3 by hydrothermal synthesis.

In Figure 24, equilibrium calculations and experimental values of the total phosphorus leached from apatites are presented. The data for Apatite 1 exceeds the total maximum phosphorus that can be leached, and considering the error margin, the dataset would fall below the maximum phosphorus concentration. Furthermore, except for Apatite 1 leached in water at pH 8.7, all values for Apatite 1 are consistently higher than the equilibrium phosphorus concentrations by 18 mmol/L or more at the corresponding pH levels.

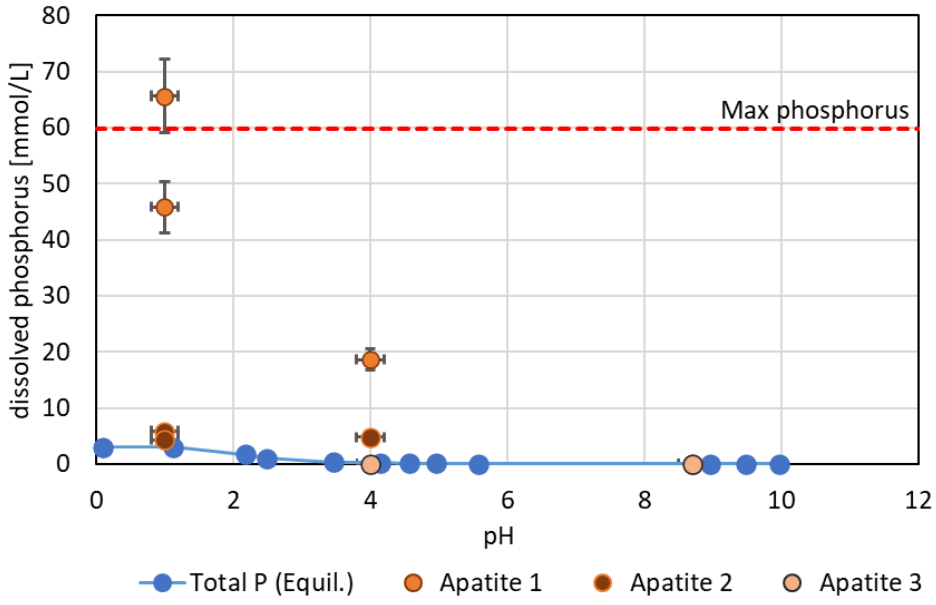

Figure 24. Equilibrium calculations of hydroxyapatites across a range of pH values. FactSage equilibrium calculations are displayed in blue, and experimental data in orange and brown colours.

SEM-EDX images were taken to identify the reasons for the differences in leaching behaviours within the identical solvents. Apatite 1 and Apatite 2 exhibit similarities in topography, while apatite 3 is different (Figure 25). This might indicate differences in the apatite structure, if it is amorphous or crystalline, and why the leaching behaviour is different, especially with apatite 2 and 3 as they should have similar leaching behaviours.

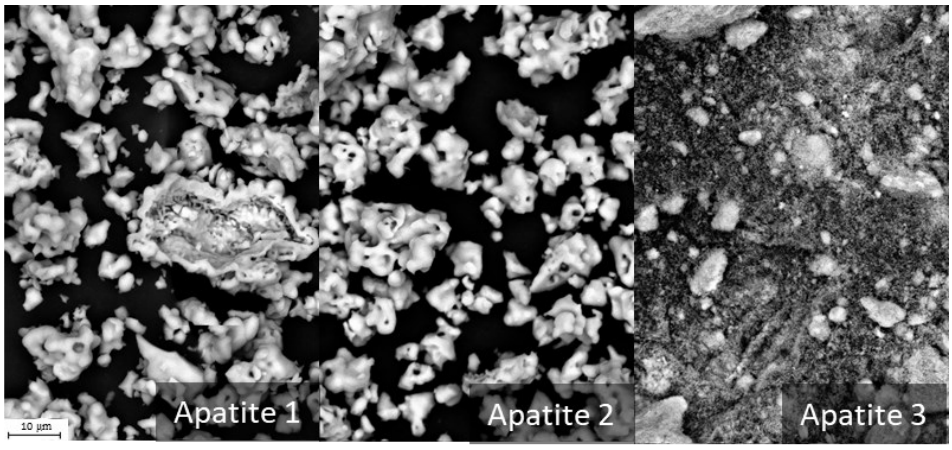

Figure 25. SEM-EDX images of Apatite 1, 2, and 3.

As discussed in Section 5.2.1, Apatite 2 and 3 were synthetised using the same method, with the only difference being the closed lid during the synthesis of Apatite 3. The need for two syntheses arose due to elevated silica levels observed in Apatite 2, not reflected in the table below. A new batch was prepared, and both reanalyzed, which revealed similar levels of silica in all apatites. The reanalyzed data for Apatite 2 is shown in the table below. While all apatites share a similar phosphorus percentage, Apatite 3 exhibited a slightly lower phosphorus content and was the only one to contain chloride. This could be due to improver washing of the sample, as the reaction included $CaCl_2$. Additionally, Apatite 3 displayed higher magnesium and lower calcium levels compared to Apatite 1 and 2. It is noteworthy that magnesium and silica were not added into the reaction, indicating that their presence is likely due to impurities acquired during the synthesis process.

Table 10. Bulk analysis results from SEM-EDX for Apatite 1, 2, and 3. All values are represented in atom percentage

Atom %

	O	Mg	Al	Si	P	Cl	Ca
Apatite 1	70.88	0.11	0	0.08	10.99	0	17.94
Apatite 2	69.29	0.16	0	0.09	11.43	0	19.02
Apatite 3	78.15	1.49	0	0.08	9.87	0.74	9.68

In conclusion, the focus was on determining the phosphorus concentration in three hydroxyapatite samples (Apatite 1, 2, and 3) synthesized using different methods. SEM-EDX images reveal difference differences in the topography of Apatite 1, 2, and 3, suggesting potential structural variations that may influence leaching behaviour. This helps with understanding the effect that the presence of hydroxyapatite might have in leaching with other phosphates or more complex samples, such as biomass ashes. Overall, while phosphorus percentages are similar, these findings highlight subtle structural and compositional differences among the hydroxyapatite samples.

6.2.4 Leaching behaviour of biomass ashes

In Table 11 the dilution factor for UV-Vis measurements is shown. For WB samples, no observable colour changes occurred, making them unmeasurable using UV-Vis spectroscopy. The next step was to calculate the dilution of the samples; both from the mixed reagent and the dilution. After determining the phosphate concentrations following the dilution adjustments, the phosphorus content was subsequently calculated from these phosphate concentrations. All the calculations and steps can be found in Appendix B. The phosphorus concentration is higher in RSC in HCl and HNO_3 compared to SSS. However, in water both leached a similar amount of phosphorus. Additionally, analyzing the same sample twice resulted in a difference in absorbance and, consequently, a varied concentration, although the values are in close proximity. It can also be seen that the use of different acids did not affect the leaching drastically, which indicates that the pH-dependent nature influenced the leaching, and not the choice of acid as an oxidizing agent.

Table 11. Dilution factors and phosphorus concentrations for biomass ash samples in different solvents

Biomass	Solvent	Dilution	mmol/L
RSC	H_2O	1:10	0.226
RSC	H_2O	1:10	0.211
RSC	HCl	1:1000	26.9
RSC	HNO_3	1:1000	28.1
SSS	H_2O	1:10	0.286
SSS	HCl	1:100	4.86
SSS	HNO_3	1:100	4.01

To assess the reliability of the MB method coupled with UV-Vis, a comparison with ICP-OES was conducted (Figure 26). The ICP-OES analysis was performed twice, with the first analysis (ICP 1) showing a slightly lower coefficient of determination than anticipated, and the second analysis (ICP 2) affected by reduced sensitivity due to a dirty sensor. A third ICP-OES analysis of the biomass ashes could not be undertaken as there was no material left. Despite this, WB was shown to have the highest amount of phosphorus leached, especially a higher concentration leached in

water compared to the other samples. Also, more phosphorus from WB was leached in water than in HCl or HNO_3. The difference between ICP 1 and ICP 2 for WB HCl and HNO_3 is around 4 mmol/L. Similarly, the difference in phosphorus concentration for RSC and SSS in UV-Vis, ICP 1 and 2 is around 1 mmol/L. The order of the biomass ashes in terms of dissolved phosphorus was WB>RSC>SSS, as determined by both UV-Vis spectroscopy and ICP-OES.

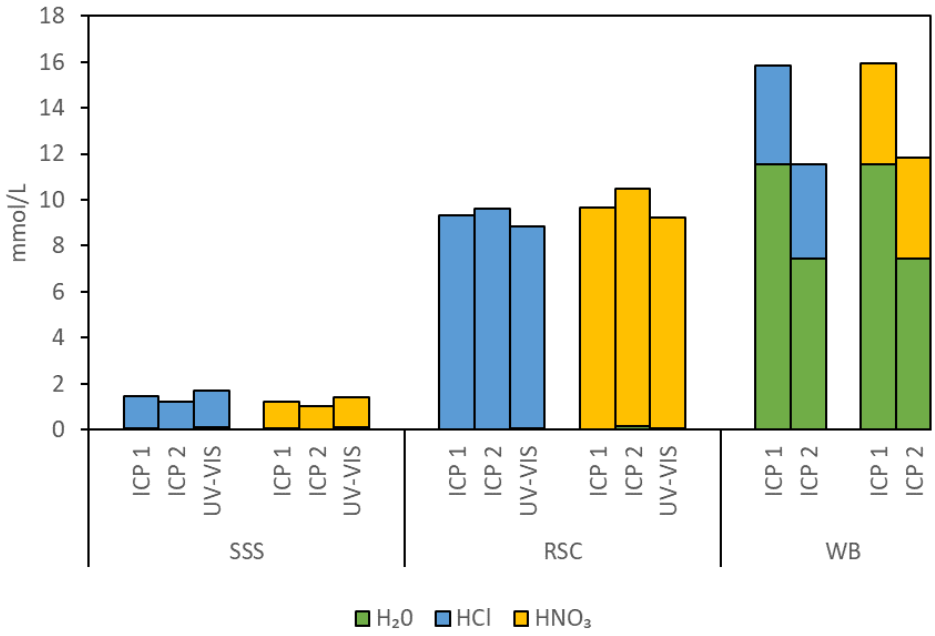

Figure 26. Concentration of phosphorus leaching from samples subjected to 50 mL H_2O and then 50 mL HCl or HNO_3 measured using ICP-OES and UV-Vis. The same samples were analyzed two times with ICP-OES. Note that results from UV-Vis were not obtained for the WB sample.

The biomass ash before leaching was also analyzed with ICP-OES (Figure 27). As mentioned earlier, the ICP-OES analysis was performed twice due to lower coefficient determination and a dirty sensor. The darker colour in Figure 27, is the analysis from ICP 1 and the lighter colour is ICP 2. Among all biomass ashes, potassium, phosphorus, aluminium, and zinc showed higher values in ICP 2 compared to ICP 1 for each respective biomass ash. On the other hand, magnesium, iron, manganese, and sodium showed higher values in ICP 1 compared to ICP 2 for each respective biomass ash. The lower value of calcium in WB could indicate that there is less of calcium phosphate, for example hydroxyapatite, which could explain why a lot of phosphorus was leached in water compared to SSS and RSC. The higher amount of iron in WB compared to SSS and RSC could interfere with the MB method, possibly contributing

to the inability to analyze WB with UV-Vis. For all biomass ashes around 15% of the total phosphorus present in the ash was leached. The observed order of phosphorus concentration in the ash before leaching aligns with the order of dissolved phosphorus from the ashes. This suggests that there was not a specific compound in a given biomass ash with significantly lower solubility compared to the other ashes.

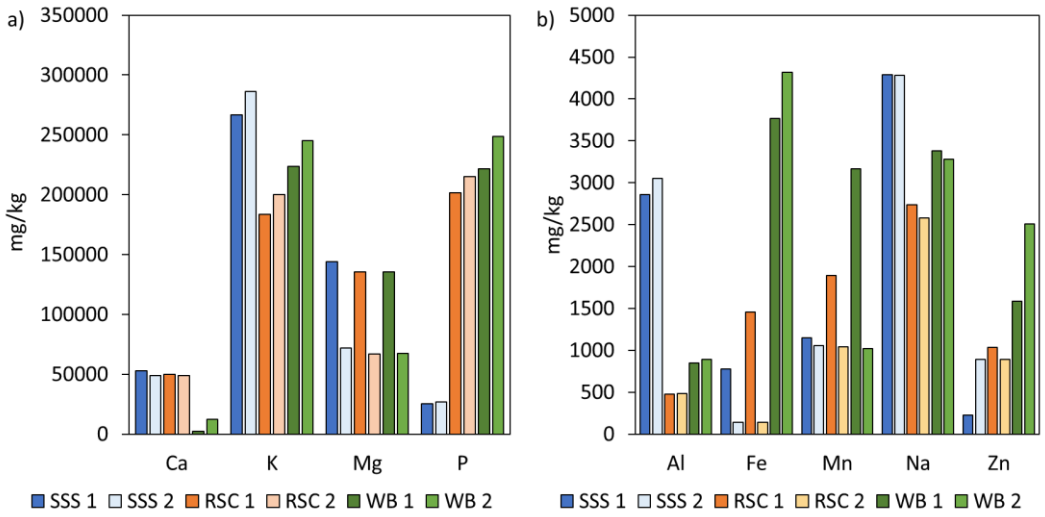

Figure 27. Elemental Composition of Biomass Samples (SSS, RSC, WB) Analyzed by ICP-OES. Values are given in mg/kg for Al, Ca, Fe, K, Mg, Mn, Na, P, and Zn. The numbers following SSS, RSC, and WB indicate whether the results are from ICP analysis 1 or 2. a) displays results for Ca, K, Mg, and P, while b) presents data for Al, Fe, Mn, Na, and Zn.

Further investigation of the composition was conducted using SEM-EDX to understand the leaching behaviour of the biomass ashes better (Table 12). It is important to note that SEM-EDX analyzes the surface only, and differences may arise compared to ICP results due to this limited depth of analysis. The lower calcium content in WB, as concluded from the ICP analysis, is consistent with the SEM-EDX findings compared to SSS and RSC. However, the iron levels among the biomass samples, as observed in SEM-EDX, show similar atom percentages, with WB having the second-highest iron content. This contrasts with the ICP-OES analysis (Figure 27), where WB appears to have the highest iron concentration, while the others exhibit only half or much less iron compared to WB. The phosphorus values for SSS, RSC, and WB align consistently with both ICP-OES and UV-Vis analyses, indicating a consistent trend in phosphorus concentration across the methods. The sulphur, which is found in SSS and RSC under 1 atom%, and the silica, found in all samples, can react with the molybdate species instead of phosphorus in the MB method and give an

inaccurate reading of the phosphorus concentration. It is possible that some of the silica originates from contamination during the process, as is impurities of other elements.

Table 12. Bulk analysis results from SEM-EDX for SSS, RSC, and WB. All values are represented in atom percentage

Atom %

	O	Al	Ca	Fe	K	M	M	Na	P	S	Si
SSS	65	0.27	9.4	0.22	14	8.2	0	0.45	1.3	0.75	0.65
RSC	69	0	6.4	0.11	7.3	5.9	0	0.24	9.8	0.89	0.2
WB	66	0	1.1	0.17	12	6.5	0.16	0.44	13	0	0.83

In conclusion, this section explored the leaching behaviour of biomass ashes, focusing on phosphorus concentration determination through UV-Vis and ICP-OES analyses. Table 11 showcased dilution factors and phosphorus concentrations, revealing distinct patterns between solvents and biomass types. The accuracy of the MB method coupled with UV-Vis was evaluated against ICP-OES. However, no clear trends emerged whether the MB method would consistently over or underestimate values with each sample. SEM-EDX provided insights into elemental composition that could affect the readings of phosphorus in the MB method. Despite differences observed in iron levels between ICP-OES and SEM-EDX, consistent trends in phosphorus concentration across methods were noted, revealing the phosphorus order as WB> RSC>SSS. The impact of iron, sulphur, and silica on phosphorus readings could be the causes of differences between the results from UV-Vis and ICP-OES.

7 Summary and Conclusions

The thesis investigated the leaching of phosphates from model chemicals and biomass ashes in different solvents. Firstly, phosphate compounds were examined to discover the leaching behaviour of single phosphates. Secondly, the leaching behaviour of hydroxyapatites were examined as it can be found in biomass ashes and therefore affects the leaching behaviour. Finally, the leaching of biomass ashes was studied to give a broader understanding of more complex samples.

The molybdenum blue method with Sb(III) and ascorbic acid as reagents was employed to investigate the leaching behaviour of various phosphates, both as individual phosphates and mixtures in solvents. These solvents were utilized to adjust the pH, demonstrating the impact on leaching. A correlation was observed between lower pH levels and increased phosphorus leaching from the phosphates, which was also seen in the equilibrium data. The observed order of solubility in the experiments was $AlPO_4 < Ca_3(PO_4)_2 < Mg_3(PO_4)_2$, consistent with the principles of hard and soft acids and bases. The equilibrium data was also utilized to investigate how well it correlated with the experimental data. Comparisons revealed that, in most cases, the experimental values closely approximated the equilibrium data obtained from Factsage. However, to validate this proximity and enhance understanding, further experimental data in varied conditions is essential.

The leaching of hydroxyapatites showed a trend with the most being leached at lower pH. As the hydroxyapatites were synthetized and leached differently, the structural variations of the hydroxyapatites, as seen in SEM-EDX images, could be the reason for the different leaching behaviours. As some biomass ashes can include hydroxyapatite, the leaching behaviour attained could explain the leaching behaviour of biomass ashes that contain calcium as it is a component in apatites.

In the analysis of phosphorus concentration in biomass ashes, the order was determined as follows: wheat bran > rapeseed cake > sunflower seed shell. With ICP-OES, it was observed that wheat bran exhibited the highest phosphorus leaching when water was used as a solvent. In contrast, for the other biomass ashes, phosphorus

leaching was predominantly observed when HCl or HNO_3 was employed as the solvent. Additionally, it was observed that excessively high HCl concentration, such as 1 M, hindered the molybdenum blue method, resulting in no colour change, while a noticeable colour change occurred with 0.1 M HCl. The choice of acid did not affect the leaching behaviour as it was pH dependant and not due to oxidizing agents in HNO_3. In the biomass samples there were elements that could cause interferences like silicate, sulphate, and iron. In the case of wheat bran, the presence of iron could be the factor preventing the efficiency of the molybdenum blue method.

Future studies should further explore the behaviours of phosphates, particularly in relation to the equilibrium data. Additionally, examining biomass ash samples using a clean ICP-OES is essential to validate the results and assess the reliability of the molybdenum blue method for future applications.

8 Swedish Summary - Svensk Sammanfattning

Den svenska titeln för avhandlingen är ”Lakning av fosfor från biomassa aska och modell kemikalier”.

Avhandlingen är indelad i tre delområden: en teoretisk del, en metoddel och en experimentell del. I den teoretiska delen diskuteras fosfor i naturen och lakning av material innehållande höga halter av fosfor. I metoddelen diskuteras alla metoder som användes för att analysera proven i den experimentella delen. Molybdenblå-metodens (eng. *Molybdenum blue method*) tillämplighet för att snabbt och kostnadseffektivt kunna analysera urlakat fosfor undersöktes. I den experimentella delen beskrivs molybden blå metoden, dess noggrannhet och mängden fosfor som lakas ur aska från biomassa i olika lösningsmedel. Lakningsbeteendet för rena enskilda fosfatföreningar undersöktes först. Sedan undersöktes lakningsbeteendet hos hydroxiapatiter, eftersom de kan hittas i askan och påverkar därför lakningsbeteendet. Slutligen studerades lakning av fosforn från aska för att ge en bredare förståelse av mer komplexa prover.

Fosfor är en viktig råvara för Europeiska unionen eftersom den används inom flera områden, exempelvis byggnadsmaterial och gödsel. I takt med att befolkningen ökar stiger behovet av livsmedel, vilket i sin tur ökar efterfrågan på gödsel. Den ökande efterfrågan väcker oro eftersom tillgången på fosforråvaror närmar sig uttömning. På grund av det har en mer hållbar källa på fosfor letats efter. Aska från förbränning av restprodukter från jordbruket och slam från avloppsvatten kan innehålla mycket fosfor och har därför väckt intresse som fosforkällor. Askan kan också innehålla tungmetaller och lämpar sig därför inte direkt för användning som gödsel. Det har lett till forskning inom avlägsnande av tungmetaller och andra skadliga ämnen ur aska. Forskningen behövs för att kunna fortsätta användningen av aska. Eftersom askan från de här källorna kan variera kraftigt i struktur och sammansättning, kan det vara utmanande att effektivt avlägsna de skadliga ämnena genom lakning. En djupare förståelse av fosfor i naturen och dess sammansättning i växter kan bidra till optimering av lakningsmetoder.

När lakning av fosfor undersöktes, testades det samtidigt en metod för kvantifiering av fosfor. Molybden blå metoden skapar en stark blå färg när en fosfatjon och

molybdenjon förenas till ett fosformolybdenblå komplex (eng. *phosphomolybdenum blue complex*). Flera olika reagenser kan användas, men den här avhandlingen fokuserar på askorbinsyra och antimon(III)-blandning. Färgförändringen mellan askorbinsyra och antimon(III)-blandningen sker på 10 minuter. Det eliminerar behovet av uppvärmningsprocedurer som krävs med andra reagenser, samtidigt som man får en stabil produkt som varar i flera timmar och inte påverkas av kloridinterferens. När en färgförändring har skett analyseras provet med UV-Vis spektrofotometer. Interferenser kan orsaka fel i mätningarna genom att binda till molybdatjonen eller hindra molybden blå reaktionen. Till exempel kan arsenat eller silikat binda till molybdatjonen i stället för fosfor. För att säkerställa noggrannheten i resultaten och identifiera potentiella interferenser användes andra analysmetoder som ICP-OES och SEM-EDX. Två analyser med ICP-OES gjordes på grund av orenheter och en tredje skulle ha behövts, men proverna hade tagit slut. Även jämviktsberäkningar gjordes med Factsage för att jämföra den teoretiska datan med den experimentella.

Det optimala koncentrationsområdet för noggranna mätningar fastställdes genom att en kalibreringskurva konstruerades med hjälp av standardlösningar, vilket visade ett detektionsområde på 1 ppm till 7 ppm vid 710 nm. Vid högre koncentrationer kunde ingen tydlig topp detekteras. De färgförändringar som observerades i prover inom intervallet 1 till 7 ppm fungerade som en praktisk referens för att avgöra om ytterligare utspädningar var nödvändiga före analys med UV-Vis spektrofotometern. Metoden användes för att först bestämma lakningsbeteendet för olika rena fosfater: $AlPO_4$, $Ca_3(PO_4)_2$ och $Mg_3(PO_4)_2$. Lösligheten av fosfatföreningar visade att AlPO4 är minst lösligt, följt av $Ca_3(PO_4)_2$ och $Mg_3(PO_4)_2$. Genom att undersöka beteendet under varierande pH med hjälp av Factsage-jämviktsberäkningar observerades det att Factsage-resultaten överensstämde generellt med löslighetstrenden från experimentella resultat, vilket förstärkte korrelationen mellan lägre pH-nivåer och ökad fosforlakning. Dessutom gav Factsage-jämviktsberäkningarna värdefulla insikter i jämviktsdata, vilket klargjorde lakningsbeteendet i olika experimentella förhållanden och förbättrade den övergripande förståelsen av fosforlakningen. Hydroxiapatitens lakningsbeteende studerades vidare vid olika pH. Först producerades hydroxiapatit på två olika sätt: kemisk fällning och hydrotermisk syntes. Det visade sig att skillnader i partikelstorleken och sammansättningen hade inverkan på lakningsbeteendet. Vid lägre pH lakades det mer fosfor, men beroende på använda syntesen lakades det olika

mängder fosfor. Dessa skillnader kan anses vara på grund av de strukturella variationer som kan ses i SEM-EDX-bilder. De här skillnaderna i topografin kan vara orsaken till de olika lakningsbeteendena. Förståelsen av hydroxiapatitens lakningsbeteende ger insikter i potentiella likheter i lakningsmönstren för kalciumrik aska från biomassa, där hydroxiapatit kan förekomma som en komponent. I undersökningen av hur fosfor lakas ur askan låg fokus på att bestämma fosforkoncentrationer med hjälp av UV-Vis- och ICP-OES-analyser. Lakningsmedel och typen av biomassa-aska hade en stor inverkan på hur mycket fosfor som lakades ur. Askor av solrosfrö skal (SSS), rapskaka (RSC), vetekärna (WB) visade att från SSS och RSC lakades det mest fosfor med syra vid pH 2. Medan WB hade största lakningen i vatten. Noggrannheten hos molybden blå metoden med UV-Vis utvärderades mot ICP-OES och resultaten överensstämde väl. Grundämnes-sammansättningen bestämdes med SEM-EDX. Biomassa-askorna innehöll bland annat olika mängder Fe, S, och Si. Dessa kan påverka fosforbestämningen med UV-Vis och orsaken till att WB inte kunde analyseras med UV-Vis. Trots avvikelser i järnnivåer mellan ICP-OES och SEM-EDX observerades en konsekvent fosforkoncentrationstrend, WB>RSC>SSS, mellan metoderna.

Sammanfattningsvis, i denna avhandling undersöktes lakningsbeteendet av fosfor från olika biomassa-askor genom att använda olika lakningsmedel. I detta arbete undersöktes fosfors lakningsbeteende allt från enskilda fosfater till att utforska hydroxiapatiter som finns i biomassaaska och slutligen studera komplexa biomassa askprover. Genom att använda molybdenblå-metoden med antimon(III) och askorbinsyra avslöjar studien pH-beroende lakningsbeteenden, vilket stöds av jämviktsdata. Resultaten med molybdenblå-metoden överensstämde väl med ICP-OES resultaten. Jämviktsberäkningarna visade god korrelation med de experimentella resultaten. Medan jämviktsdata nästan motsvarar experimentella värdena kan det ännu undersökas vidare för att få ett heltäckande förståelse av fosforlakning. Dessutom är det viktigt att undersöka askprover från biomassa med en ren ICP-OES för att validera resultaten och bedöma tillförlitligheten hos molybden blå metoden för framtida tillämpningar.

9 References

(1) European Commission. *Critical raw materials*. https://single-market-economy.ec.europa.eu/sectors/raw-materials/areas-specific-interest/critical-raw-materials_en (accessed 2023-09-12).

(2) FAO. *World Fertilizer Trends and Outlook to 2022*; Rome, 2019.

(3) Baffes, J.; Chian Koh, W. *Soaring fertilizer prices add to inflationary pressures and food security concerns*. https://blogs.worldbank.org/opendata/soaring-fertilizer-prices-add-inflationary-pressures-and-food-security-concerns (accessed 2023-07-26).

(4) Baffes, J.; Chian Koh, W. *Fertilizer prices ease but affordability and availability issues linger*. https://blogs.worldbank.org/opendata/fertilizer-prices-ease-affordability-and-availability-issues-linger (accessed 2023-07-26).

(5) The Editors of Encyclopaedia Britannica. Phosphorus. *Encyclopedia Britannica*; 2023.

(6) Tan, Z.; Lagerkvist, A. Phosphorus Recovery from the Biomass Ash: A Review. *Renew. Sustain. Energy Rev.* **2011**, *15* (8), 3588–3602. https://doi.org/10.1016/j.rser.2011.05.016.

(7) Brownlie, W. J.; Sutton, M. A.; Heal, K. V.; Reay, D. S.; Spears, B. M. *Chapter 1. Our Phosphorus Future - an Introduction*; Brownlie, W. J., Sutton, M. A., Heal, K. V., Reay, D. S., Spears, B. M., Series Eds.; UK Centre for Ecology & Hydrology: Edinburgh, 2022. doi: 10.13140/RG.2.2.32933.58085 (accessed 2023-07-27).

(8) Hassoun, J.; Bonaccorso, F.; Agostini, M.; Angelucci, M.; Betti, M. G.; Cingolani, R.; Gemmi, M.; Mariani, C.; Panero, S.; Pellegrini, V.; Scrosati, B. An Advanced Lithium-Ion Battery Based on a Graphene Anode and a Lithium Iron Phosphate Cathode, 2014. https://doi.org/10.1021/nl502429m (accessed 2023-07-27).

(9) Sun, H.; Xu, X.; Yan, Z.; Chen, X.; Cheng, F.; Weiss, P. S.; Chen, J. Porous Multishelled Ni2P Hollow Microspheres as an Active Electrocatalyst for Hydrogen and Oxygen Evolution. *Chem. Mater.* **2017**, *29* (19), 8539–8547. https://doi.org/10.1021/acs.chemmater.7b03627.

(10) *Mineral Commodity Summaries 2023*; U.S. Geological Survey, 2023; pp 132–133. https://doi.org/10.3133/mcs2023.

(11) Cordell, D.; Drangert, J.-O.; White, S. The Story of Phosphorus: Global Food Security and Food for Thought. *Glob. Environ. Change* **2009**, *19* (2), 292–305. https://doi.org/10.1016/j.gloenvcha.2008.10.009.

(12) Pitman, R. M. Wood Ash Use in Forestry – a Review of the Environmental Impacts. *For. Int. J. For. Res.* **2006**, *79* (5), 563–588. https://doi.org/10.1093/forestry/cpl041.

(13) Pettersson, A.; Åmand, L.-E.; Steenari, B.-M. Leaching of Ashes from Co-Combustion of Sewage Sludge and Wood—Part I: Recovery of Phosphorus. *Biomass Bioenergy* **2008**, *32* (3), 224–235. https://doi.org/10.1016/j.biombioe.2007.09.016.

(14) Franz, M. Phosphate Fertilizer from Sewage Sludge Ash (SSA). *Waste Manag.* **2008**, *28* (10), 1809–1818. https://doi.org/10.1016/j.wasman.2007.08.011.

(15) Richardson, J. F.; Harker, J. H.; Backhurst, J. R. Leaching. In *Chemical Engineering*; Chemical Engineering Series; Butterworth-Heinemann: Oxford, 2002; Vol. 2, pp 502–541. https://doi.org/10.1016/B978-0-08-049064-9.50021-7.

(16) Herzel, H.; Krüger, O.; Hermann, L.; Adam, C. Sewage Sludge Ash — A Promising Secondary Phosphorus Source for Fertilizer Production. *Sci. Total Environ.* **2016**, *542*, 1136–1143. https://doi.org/10.1016/j.scitotenv.2015.08.059.

(17) Leng, L.; Bogush, A. A.; Roy, A.; Stegemann, J. A. Characterisation of Ashes from Waste Biomass Power Plants and Phosphorus Recovery. *Sci. Total Environ.* **2019**, *690*, 573–583. https://doi.org/10.1016/j.scitotenv.2019.06.312.

(18) Sevonius, C.; Yrjas, P.; Lindberg, D.; Hupa, L. Agglomeration Tendency of a Fluidized Bed during Addition of Different Phosphate Compounds. *Fuel* **2020**, *268* (117300). https://doi.org/10.1016/j.fuel.2020.117300.

(19) Zumdahl, S. S.; Zumdahl, S. A. *Chemistry*, 7th ed.; Houghton Mifflin Company: Boston, MA, U.S.A, 2007.

(20) Mackey, K. R. M.; Paytan, A. Phosphorus Cycle. In *Encyclopedia of Microbiology*; Schaechter, M., Ed.; Academic Press: Oxford, 2009; pp 322–334. https://doi.org/10.1016/B978-012373944-5.00056-0.

(21) Schipanski, M. E.; Bennett, E. M. The Phosphorus Cycle. In *Fundamentals of Ecosystem Science*; Weathers, K. C., Strayer, D. L., Likens, G. E., Eds.; Academic Press, 2021; pp 189–213. https://doi.org/10.1016/B978-0-12-812762-9.00009-5.

(22) Ribot, C.; Wang, Y.; Poirier, Y. Expression Analyses of Three Members of the AtPHO1 Family Reveal Differential Interactions between Signaling Pathways Involved in Phosphate Deficiency and the Responses to Auxin, Cytokinin, and Abscisic Acid. *Planta* **2008**, *227* (5), 1025–1036. https://doi.org/10.1007/s00425-007-0677-x.

(23) Havlin, J. L.; Tisdale, S. L.; Nelson, W. L.; Beaton, J. D. *Soil Fertility and Fertilizers*, 8th ed.; Pearson Education India, 2016.

(24) Dissanayaka, D. M. S. B.; Ghahremani, M.; Siebers, M.; Wasaki, J.; Plaxton, W. C. Recent Insights into the Metabolic Adaptations of Phosphorus-Deprived Plants. *J. Exp. Bot.* **2021**, *72* (2), 199–223. https://doi.org/10.1093/jxb/eraa482.

(25) Gasser, M. S.; Ismail, Z. H.; Abu Elgoud, E. M.; Hai, F. A.; Ali, I. O.; Aly, H. F. Alkali Treatment–Acid Leaching of Rare Earth Elements from Phosphogypsum Fertilizer: Insight for Additional Resource of Valuable Components. *BMC Chem.* **2022**, *16* (1), 51. https://doi.org/10.1186/s13065-022-00845-7.

(26) Gupta, N.; Gedam, V. V.; Moghe, C.; Labhasetwar, P. Investigation of Characteristics and Leaching Behavior of Coal Fly Ash, Coal Fly Ash Bricks and Clay Bricks. *Environ. Technol. Innov.* **2017**, *7*, 152–159. https://doi.org/10.1016/j.eti.2017.02.002.

(27) Shahbaz, A. A Systematic Review on Leaching of Rare Earth Metals from Primary and Secondary Sources. *Miner. Eng.* **2022**, *184* (107632). https://doi.org/10.1016/j.mineng.2022.107632.

(28) Fang, L.; Li, J.; Guo, M. Z.; Cheeseman, C. R.; Tsang, D. C. W.; Donatello, S.; Poon, C. S. Phosphorus Recovery and Leaching of Trace Elements from Incinerated Sewage Sludge Ash (ISSA). *Chemosphere* **2018**, *193*, 278–287. https://doi.org/10.1016/j.chemosphere.2017.11.023.

(29) Biswas, B. K.; Inoue, K.; Harada, H.; Ohto, K.; Kawakita, H. Leaching of Phosphorus from Incinerated Sewage Sludge Ash by Means of Acid Extraction Followed by Adsorption on Orange Waste Gel. *J. Environ. Sci.* **2009**, *21* (12), 1753–1760. https://doi.org/10.1016/S1001-0742(08)62484-5.

(30) Kuligowski, K.; Poulsen, T. G. Phosphorus and Zinc Dissolution from Thermally Gasified Piggery Waste Ash Using Sulphuric Acid. *Bioresour. Technol.* **2010**, *101* (14), 5123–5130. https://doi.org/10.1016/j.biortech.2010.01.143.

(31) Yoshizaki, S.; Tomida, T. Principle and Process of Heavy Metal Removal from Sewage Sludge. *Environ. Sci. Technol.* **2000**, *34* (8), 1572–1575. https://doi.org/10.1021/es990979s.

(32) NareshKumar, R.; Nagendran, R. Changes in Nutrient Profile of Soil Subjected to Bioleaching for Removal of Heavy Metals Using Acidithiobacillus Thiooxidans. *J. Hazard. Mater.* **2008**, *156* (1–3), 102–107. https://doi.org/10.1016/j.jhazmat.2007.12.001.

(33) Houck, M. M.; Siegel, J. A. Light and Matter. In *Fundamentals of Forensic Science*; Houck, M. M., Siegel, J. A., Eds.; Academic Press: San Diego, 2015; pp 93–119. https://doi.org/10.1016/B978-0-12-800037-3.00005-4.

(34) Worsfold, P. J. Spectrophotometry | Overview. In *Encyclopedia of Analytical Science*; Worsfold, P., Townshend, A., Poole, C., Eds.; Elsevier: Oxford, 2005; pp 318–321. https://doi.org/10.1016/B0-12-369397-7/00714-7.

(35) Harvey, D. Ultraviolet-Visible and Infrared Spectrophotometry. In *Modern Analytical Chmeistry*; James M. Smith, 2000; pp 388–412.

(36) Hitachi High-Tech Corporation. *8. Structure of a spectrophotometer (3)*. Hitachi High-Tech Corporation. https://www.hitachi-hightech.com/global/en/knowledge/analytical-systems/spectrophotometers/uv/basics/course8.html (accessed 2023-06-26).

(37) Nagul, E. A.; McKelvie, I. D.; Worsfold, P.; Kolev, S. D. The Molybdenum Blue Reaction for the Determination of Orthophosphate Revisited: Opening the Black Box. *Anal. Chim. Acta* **2015**, *890*, 60–82. https://doi.org/10.1016/j.aca.2015.07.030.

(38) Worsfold, P. J.; Gimbert, L. J.; Mankasingh, U.; Omaka, O. N.; Hanrahan, G.; Gardolinski, P. C. F. C.; Haygarth, P. M.; Turner, B. L.; Keith-Roach, M. J.; McKelvie, I. D. Sampling, Sample Treatment and Quality Assurance Issues for the Determination of Phosphorus Species in Natural Waters and Soils. *Talanta* **2005**, *66* (2), 273–293. https://doi.org/10.1016/j.talanta.2004.09.006.

(39) Keggin, J. F. Structure and Formula of 12-Phosphotungstic Acid. *Proc. R. Soc. Lond.* **1934**, *144*, 75–100.

(40) Pai, S.-C.; Wang, T.-Y. Effect of Heating on the Color Formation Reaction in the Murphy and Riley Method for the Determination of Phosphate in Natural Waters. *J. Environ. Anal. Chem.* **2015**, *2* (3). https://doi.org/10.4172/2380-2391.1000139.

(41) Majumdar, A. J.; Dubey, N. Applications of Inductively Coupled Plasma-Atomic Emission Spectrometry (ICP-OES) in Impurity Profiling of Pharmaceuticals. *Int. J. Pharm. Life Sci.* **2017**, *8* (1), 5420–5425.

(42) Khan, S. R.; Sharma, B.; Chawla, P. A.; Bhatia, R. Inductively Coupled Plasma Optical Emission Spectrometry (ICP-OES): A Powerful Analytical Technique for Elemental Analysis. *Food Anal. Methods* **2022**, *15* (3), 666–688. https://doi.org/10.1007/s12161-021-02148-4.

(43) Ul-Hamid, A. Introduction. In *A Beginners' Guide to Scanning Electron Microscopy*; Springer International Publishing AG: Cham, Switzerland, 2018; pp 1–14.

(44) Bale, C. W.; Bélisle, E.; Chartrand, P.; Decterov, S. A.; Eriksson, G.; A. E. Gheribi; Hack, K.; Kang, Y.-B.; Melançon, J.; Pelton, A. D.; Petersen, S.; Robelin, C.; Sangster, J.; Spencer, P.; Van Ende, M.-A. Reprint of: FactSage Thermochemical Software and Databases, 2010–2016. *Calphad* **2016**, *55*, 1–19.

(45) Sokolenko, E. The Equilib Module, 2021. https://www.crct.polymtl.ca/fact/factsage/EquiSage.pdf.

(46) Andrade Neto, A. S.; Secchi, A. R.; Capron, B. D. O.; Rocha, A.; Loureiro, L. N.; Ventura, P. R. Development of a Predictive Emissions Monitoring System Using Hybrid Models with Industrial Data. In *Computer Aided Chemical Engineering*; Montastruc, L., Negny, S., Eds.; 32 European Symposium on Computer Aided Process Engineering; Elsevier, 2022; Vol. 51, pp 1387–1392. https://doi.org/10.1016/B978-0-323-95879-0.50232-0.

(47) Yelten-Yilmaz, A.; Yilmaz, S. Wet Chemical Precipitation Synthesis of Hydroxyapatite (HA) Powders. *Ceram. Int.* **2018**, *44* (8), 9703–9710. https://doi.org/10.1016/j.ceramint.2018.02.201.

(48) Zhang, G.; Chen, J.; Yang, S.; Yu, Q.; Wang, Z.; Zhang, Q. Preparation of Amino-Acid-Regulated Hydroxyapatite Particles by Hydrothermal Method. *Mater. Lett.* **2011**, *65* (3), 572–574. https://doi.org/10.1016/j.matlet.2010.10.078.

(49) Colorimetric-Analysis-of-P-A2-20.Pdf. https://www.dgtresearch.com/detailed-user-guides/Colorimetric-analysis-of-P-A2-20.pdf (accessed 2023-12-05).

(50) Pearson, R. G. Hard and Soft Acids and Bases, HSAB, Part 1: Fundamental Principles. *J. Chem. Educ.* **1968**, *45* (9), 581. https://doi.org/10.1021/ed045p581.

10 Appendix

10.1 Appendix A

UV-VIS spectrophotometer spectra

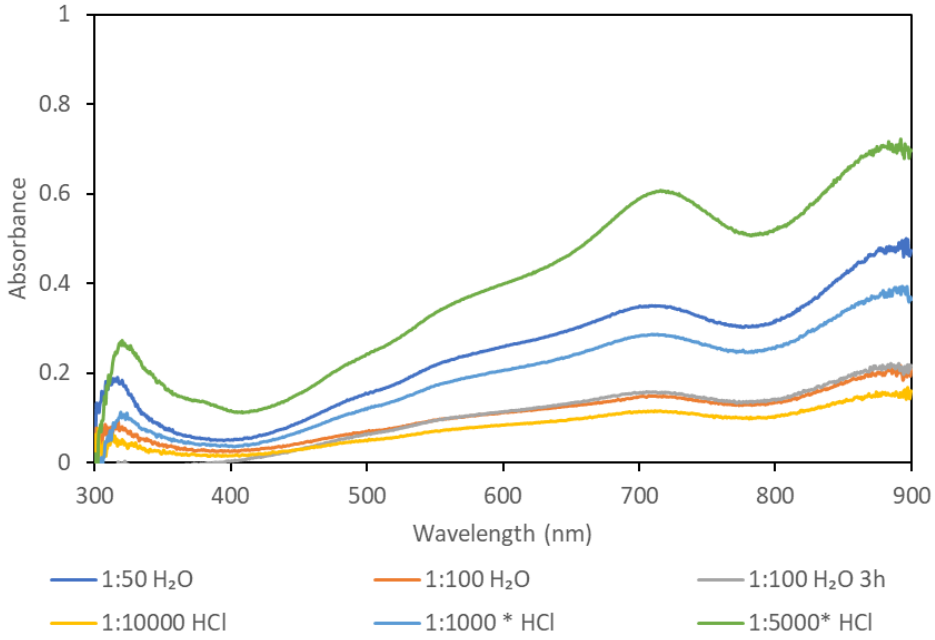

Figure A 1. UV-Vis spectra of $AlPO_4$ samples in water, pH 4 and HCl in different dilutions. Samples 1:100 H_2O (orange) and 1:100 3h H_2O (grey) are near each other and therefore might be hard to see.

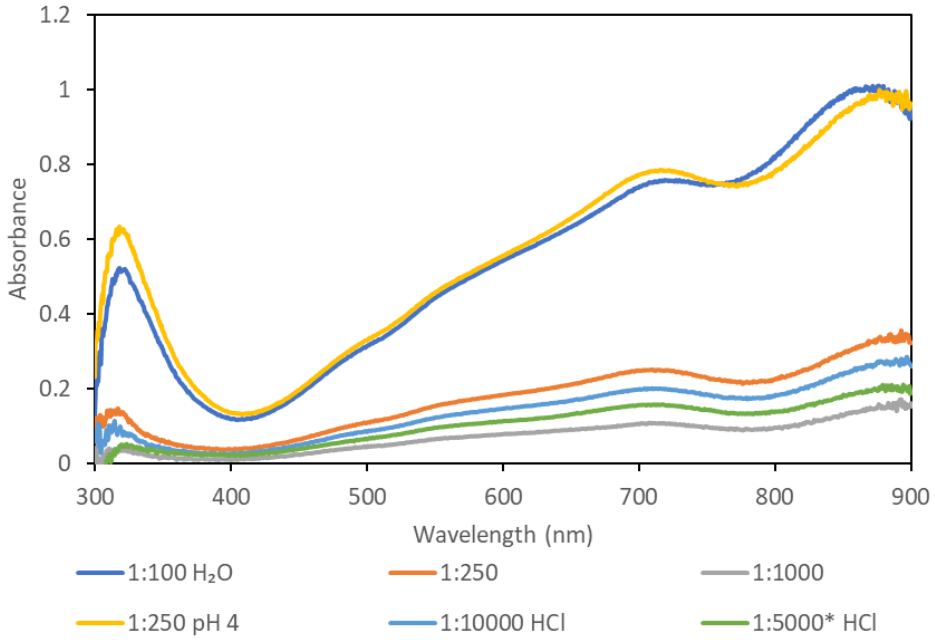

Figure A 2. UV-Vis spectra of Mg3(PO4)2 samples in water, pH 4 and HCl in different dilutions.

10.2 Appendix B

Calculations of phosphorus concentration from measurements from UV-Vis

With the absorbance obtained from the MB method using UV-Vis, phosphorus concentration can be calculated through a series of five equations. The absorbance, obtained from standard solutions for constructing a calibration curve (see Section 6.1 Construction of the calibration curve), is correlated with the concentration of the measured sample. This correlation is expressed by the formula:

$$Conc._{after\ MB\ dilution} = (Abs - b)/a$$

Equation B 1. Concentration of the measured sample.

The concentration obtained corresponds to the diluted samples, requiring further calculation to determine the correct concentration before the addition of the mixed reagent from the MB method. The first step involves accounting for the dilution caused by the molybdenum blue method. The dilution from the MB method is achieved by either adding 2 ml to a 10 ml sample or 1 ml to a 5 ml sample.

$$Conc._{before\ MB\ dilution} = Conc._{after\ MB\ dilution} \times \frac{Volume_{sample+mixed\ reagent}}{Volume_{sample}}$$

Equation B 2. Concentration before the MB dilution.

Subsequently, the concentration before other dilutions is determined using the formula:

$$Conc._{before\ dilutions} = Conc._{before\ MB\ dilution} \times Dilution\ factor_{from\ MB}$$

Equation B 3. Concentration before dilutions.

To calculate the concentration before dilution for phosphates:

$$Conc._{before\ dilution\ (phopshates)} = Conc._{before\ MB\ dilution} \times Dilution\ factor$$

Equation B 4. Concentration before dilution (phosphates).

It's important to note that the MB method provides the concentration for phosphates. Therefore, Equation B 4 gives the concentration results for phosphates, and Equation B 5 calculates the corresponding phosphorus concentration from the phosphate ions:

$$Conc._{before\ diluton\ (phosphorus)} = Conc._{before\ dilution(phosphates)} \times \frac{M_P}{M_{PO_4^{-3}}}$$

Equation B 5. Concentration before dilution (phosphorus)

Finally, the overall concentration of phosphorus is calculated:

$$Conc._{phosphorus} = \frac{Conc._{before\ diluton\ (phosphorus)}}{M_P}$$

Equation B 6. Concentration of phosphorus in mmol/L.

All the values for each calculation can be found in Table B 1 with the final concentration of phosphorus in the sample found as mmol/L.

*Table B 1. Phosphorus concentrations in various samples. Concentrations are measured in mmol/L for 500 mg in 50 or 100 mL solvent, with corresponding ppm, absorbance (abs), and dilution values presented for each sample. Results with absorbance values below 0.1 or or above 1.0, coloured in orange, are not within the reliable detection range of the UV-Vis spectrophotometer and thus excluded from the analysis. These values are mentioned for completeness in this table but are not included in the main body of the thesis. Samples diluted with 5 mL sample and 1 mL mixed reagent are marked with *.*

Sample	Abs	Conc. after MB dilution	Conc. before MB dilution	Conc. before dilution (Phosphates mg/L)	Conc. before dilution (Phosphorus mg/L)	Conc. phosphorus in mmol/L
Al 1:100 H_2O	0,15	1,06	1,27	126,9	41,4	1,34
Al 1:100 H_2O 3h	0,16	1,14	1,37	136,7	44,6	1,44
Al 1:50 H_2O	0,15	1,06	1,27	63,4	20,7	0,668
Al 1:10 H_2O	1,05	8,06	9,67	96,7	31,5	1,02
Al 1:50 pH 4	0,07	0,43	0,51	25,6	8,34	0,269
Al 1:1000 0,1M HCl*	0,29	2,11	0,34	342,5	112	3,61
Al 1:1000 0,1M HCl	0,07	0,46	0,55	549,9	179	5,79
Al 1:5000 0,1M HCl *	0,60	4,43	0,72	3614,0	1179	38,1
Al 1:10000 0,1M HCl	0,12	0,81	0,97	9749,2	3179	103
Ca 1:1000 H_2O	0,00	-0,07	-0,08	-82,6	-26,9	-0,870

Ca 1:100 H_2O	0,22	1,59	1,91	190,7	62,2	2,01
Ca 1:100 H_2O 3h	0,13	0,91	1,10	109,5	35,7	1,15
Ca 1:50 H_2O	0,35	2,61	3,13	156,3	51,0	1,65
Ca 1:50 pH 4	0,88	6,71	8,05	402,5	131	4,24
Ca 1:1000 0,1M HCl *	0,73	5,40	0,88	880,2	287	9,27
Ca 1:1000 0,1M HCl	0,35	2,62	3,14	3144,8	1026	33,1
Mg 1:1000 H_2O	0,11	0,76	0,91	911,0	297	9,59
Mg 1:1000 H_2O 3h	0,04	0,23	0,28	276,3	90,1	2,91
Mg 1:250 H_2O	0,25	1,84	2,21	551,4	180	5,81
Mg 1:100 H_2O	0,75	5,76	6,91	691,2	225	7,28
Mg 1:250 pH 4	0,78	5,97	7,16	1789,6	584	18,8
Mg 1:5000 0,1M HCl*	0,16	1,16	0,19	942,5	307	9,92
Mg 1:10000 0,1M HCl	0,20	1,47	1,76	17622,9	5747	186
Al+Ca 1:10 H_2O*	0,38	2,78	3,34	33,4	10,9	0,351
Al+Ca 1:50 H_2O*	0,09	0,67	0,81	40,4	13,2	0,425
Al+Mg 1:50 H_2O*	0,89	6,52	7,82	391,2	128	4,12
Al+Mg 1:100 H_2O*	0,53	3,89	4,67	466,9	152	4,92
Ca+Mg 1:100 H_2O*	0,29	2,10	2,52	252,5	82,3	2,66
Al+Ca 1:500 0,1M HC*	0,87	6,38	1,04	520,5	170	5,48
Al+Ca 1:1000 0.1M HCl*	0,49	3,58	0,58	583,4	190	6,14
Al+Mg 1:1000 0.1M HCl*	0,46	3,38	0,55	550,2	179	5,79
Ca+Mg 1:1000 0.1M HCl*	0,73	5,40	0,88	880,5	287	9,27
2 ppm H_2O	0,142	2,00	4,80	480	0,48	0,0155
2 ppm H_2O + HCl	0,142	1,98	4,76	476	0,48	0,0154
2 ppm HCl	0,136	1,90	4,56	456	0,46	0,0147
5 ppm H_2O	0,351	5,00	12,00	1200	1,20	0,0387
5 ppm H_2O + HCl	0,352	5,02	12,05	1205	1,20	0,0389
5 ppm HCl	0,353	5,03	12,08	1208	1,21	0,0390
RSC 2:20 H_2O #1	0,23	1,79	2,14	21,4	6,99	0,226
RSC 2:20 H_2O #2	0,21	1,67	2,00	20,0	6,53	0,211
RSC 1:1000 HCl	0,27	2,13	2,56	2556,3	834	26,9

RSC 1:1000 HNO_3	0,29	2,22	2,66	2664,6	869	28,1
SSS 1:10 H_2O	0,29	2,27	2,72	27,2	8,87	0,286
SSS 1:100 HCl	0,50	3,85	4,62	461,6	151	4,86
SSS 1:100 HNO_3	0,41	3,17	3,81	380,7	124	4,01
Apatite H_2O*	0,09	0,76	0,91	0,9	0,297	0,00960
Apatite pH4 1:1000*	0,19	1,47	1,77	1766,9	576	18,6
Apatite HCl 1:1000*	0,68	5,20	6,24	6235,2	2033	65,7
Apatite HNO_3 1:1000*	0,47	3,63	4,35	4353,5	1420	45,8
Apatite 2 H_2O*	0,09	0,83	0,99	0,99	0,324	0,0105
Apatite 2 pH4*	0,48	3,77	4,52	452	147	4,76
Apatite 2 HCl*	0,04	0,46	0,55	552	180	5,81
Apatite 2 HNO_3*	0,03	0,34	0,41	408	133	4,30
Apatite 3 H_2O*	0,46	3,40	0,55	0,55	0,180	0,00583
Apatite 3 pH4*	0,58	4,24	0,69	0,69	0,225	0,00727